Journal of Volcanology and Geothermal Research 341 (2017) 172–186

Contents lists available at ScienceDirect

Journal of Volcanology and Geothermal Research

journal homepage: www.elsevier.com/locate/jvolgeores

Sr- and Nd- isotope variations along the Pleistocene San Pedro – Linzor volcanic chain, N. Chile: Tracking the influence of the upper crustal Altiplano-Puna Magma Body

Benigno Godoy [a,*], Gerhard Wörner [b], Petrus Le Roux [c], Shanaka de Silva [d], Miguel Ángel Parada [a], Shoji Kojima [e], Osvaldo González-Maurel [f], Diego Morata [a], Edmundo Polanco [g,1], Paula Martínez [a,2]

[a] Centro de Excelencia en Geotermia de los Andes (CEGA), Departamento de Geología, Facultad de Ciencas Físicas y Matemáticas, Universidad de Chile, Plaza Ercilla 803, Santiago, Chile
[b] Abteilung Geochemie, GZG, Göttingen Universität, Goldschmidtstraße 1, Göttingen 37077, Germany
[c] Department of Geological Sciences, University of Cape Town, Rondebosch 7701, South Africa
[d] College of Earth, Ocean, and Atmospheric Sciences, Oregon State University, Corvallis, OR 97331, USA
[e] Departamento de Ciencias Geológicas, Universidad Católica del Norte, Avenida Angamos 0610, Antofagasta, Chile
[f] Programa de Doctorado en Ciencias, Mención Geología. Departamento de Ciencias Geólogicas, Universidad Católica del Norte, Avenida Angamos 0610, Antofagasta, Chile
[g] Energía Andina S.A. Cerro El Plomo 5630, Las Condes, Santiago, Chile

ARTICLE INFO

Article history:
Received 13 January 2017
Received in revised form 29 May 2017
Accepted 29 May 2017
Available online 31 May 2017

Keywords:
San Pedro – Linzor volcanic chain (SPLVC)
Altiplano-Puna Magma Body (APMB)
Isotopic shift
Geochronology

ABSTRACT

Subduction-related magmas that erupted in the Central Andes during the past 10 Ma are strongly affected by crustal assimilation as revealed by an increase in $^{87}Sr/^{86}Sr$ isotope ratios with time that in turn are correlated with increased crustal thickening during the Andean orogeny. However, contamination is not uniform and can be strongly influenced locally by crustal composition, structure and thermal condition. This appears to be the case along the NW-SE San Pedro - Linzor volcanic chain (SPLVC) in northern Chile, which straddles the boundary of a major zone of partial melt, the Altiplano_Puna Magma Body (APMB). Herein we report $^{40}Ar/^{39}Ar$ ages, compositional and isotope data on lavas from the SPLVC that track the influence of this zone of partial melting on erupted lavas with geochronological and geochemical data. Ages reported here indicate that SPLVC has evolved in the last 2 M.y., similar to other volcanoes of the Western Cordillera (e.g. Lascar, Uturuncu, Putana). $^{87}Sr/^{86}Sr$ ratios increase systematically along the chain from a minimum value of 0.7057 in San Pedro dacites to a maximum of 0.7093–0.7095 for the Toconce and Cerro de Leon dacites in the SE. These changes are interpreted to reflect the increasing interaction of SPLVC parental magmas with partial melt within the APMB eastwards across the chain. The $^{87}Sr/^{86}Sr$ ratio and an antithetic trend in $^{143}Nd/^{144}Nd$ is therefore a proxy for the contribution of melt from the APMB beneath this volcanic chain.
Similar $^{87}Sr/^{86}Sr$ increases and $^{143}Nd/^{144}Nd$ decreases are observed in other transects crossing the boundary of the APMB. Such trends can be recognized from NW to SE between Aucanquilcha, Ollagüe, and Uturuncu volcanoes, and from Lascar volcano to the N-S-trending Putana-Sairecabur-Licancabur volcanic chain to the north. We interpret these isotopic trends as reflecting different degrees of interaction of mafic parental melts with the APMB. High $^{87}Sr/^{86}Sr$, and low $^{143}Nd/^{144}Nd$ reveal zones where the APMB is thicker (~20 km) and more melt-dominated (~25% vol. partial melt) while lower $^{87}Sr/^{86}Sr$, and higher $^{143}Nd/^{144}Nd$ reveal thinner marginal zones of the APMB where lower contents of partial melt (<10% vol) involves reduced interactions. The lowest Sr-isotope ratios, and higher Nd-isotope ratios (where available) occur in magmas erupted outside the APMB (e.g. San Pedro, Lascar and Aucanquilcha volcanoes), indicating a diminished influence of crustal partial melts on parental mafic magmas. These geochemical parameters provide a useful tracer for the extent and significance of crustal partial melt bodies in magma genesis in the Central Andes.

1. Introduction

While it is known that most magma at subduction zones is generated by flux melting in the asthenospheric wedge (Tatsumi et al., 1983; Grove et al., 2012), in continental magmatic arcs, the role of the crust in controlling the evolution of even the most mafic magmas is clear

* Corresponding author.
E-mail address: bgodoy@ing.uchile.cl (B. Godoy).
[1] Present address: Servicio Nacional de Geología y Minería, Avenida Santa María 0104, Providencia, Santiago, Chile.
[2] Present address: Advanced Mining Technology Center, Avenida Tupper 2007, Santiago, Chile.

http://dx.doi.org/10.1016/j.jvolgeores.2017.05.030
0377-0273/

(e.g. Davidson et al., 1990). This is most obvious in arcs built on thick continental crust such as the Central Volcanic Zone (CVZ) of the Andes. Arc migration and crustal thickening to 70 km in the Central Andes are well documented (e.g. Scheuber and Giese, 1999; Scheuber and Reutter, 1992, Beck et al., 1996; Allmendinger et al., 1997; Kay and Mpodozis, 2001; Oncken et al., 2006; Hartley et al., 2007; Kley et al., 1999; Kley and Monaldi, 1998) and have been related to the systematic spatio-temporal changes in the geochemical and isotopic composition of erupted lavas during the last 26 M.y. (e.g. Haschke, 2002; Kay et al., 2005; Haschke et al., 2006; Mamani et al., 2008, 2010). Volcanic rocks of earlier stages of Central Andean evolution traversed thin crust and are consistently low in Sr/Y, La/Yb, and Sm/Yb ratios, whereas progressively younger magmatic products show increases in the maximum Sr/Y, La/Yb, and Sm/Yb ratios. These changes in the geochemical signature of lavas were attributed to the increasing role of garnet as a stable residual phase in magma processing within a progressively thicker Central Andean crust. This is in line with the more radiogenic signatures of the magmatism with time that are attributed to increased crustal assimilation (Rogers and Hawkesworth, 1989; Kay and Mpodozis, 2001; Davidson et al., 1990; Haschke, 2002; Haschke et al., 2006; Mamani et al., 2008, 2010).

A dominant feature of the Neogene history of the Central Andes is one the most extensive ignimbrite plateaus on Earth, the Neogene Central Andean Ignimbrite Province (Coira et al., 1982; de Silva and Francis, 1991; Trumbull et al., 2006; Salisbury et al., 2011; Freymuth et al., 2015; Brandmeier and Wörner, 2016). The most intense activity produced the Altiplano-Puna Volcanic Complex (APVC, de Silva, 1989), a volcano-tectonic province in the Central Andes occupying the high plateau between 21° and 24°S (Fig. 1). The area of the APVC coincides with the surface projection of a low-velocity zone, interpreted as a partially-molten body within the upper crust (~15 to 30 km), the so-called "Altiplano-Puna Magma Body" (AMPB; Chmielowski et al., 1999; Zandt et al., 2003; Ward et al., 2014)(Fig. 1). This body has also been recognized by electrical, gravity, and isostatic anomalies (Schilling et al., 1997; Haberland and Rietbrock, 2001; Schilling and Partzsch, 2001; Brasse et al., 2002; Schnurr et al., 2007; Prezzi et al., 2009), and is interpreted as an incrementally constructed, upper-crustal batholith (de Silva and Gosnold, 2007; Kern et al., 2016) atop an upper crustal MASH zone (Burns et al., 2015; Ward et al., 2014).

Tracking the influence of this partially molten upper crustal batholith on magma compositions in arc front volcanism is our aim in this study. The hypothesis is that crustal partial melts will be more

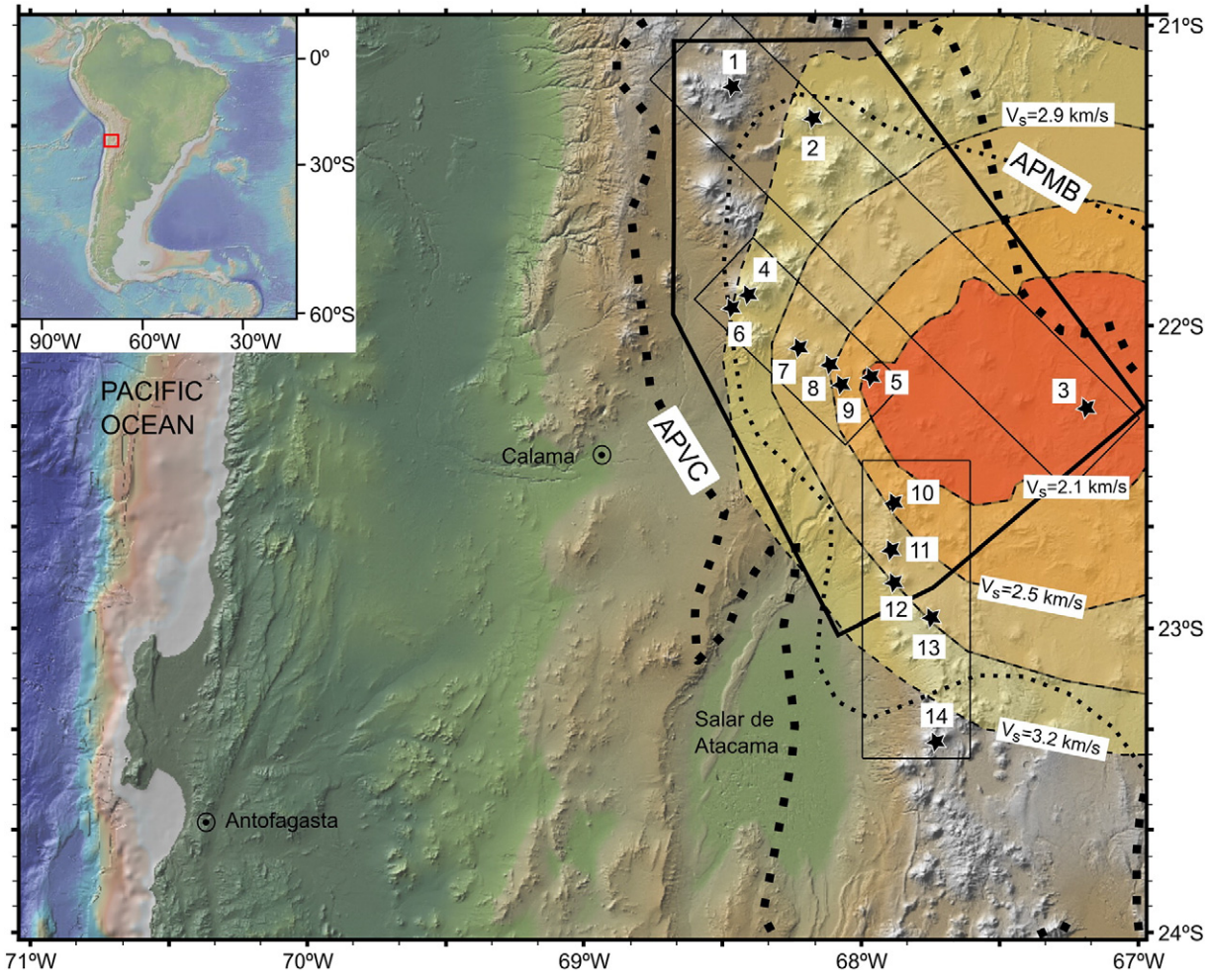

Fig. 1. Global Multi-Resolution Topography image showing location of the volcanic structures (black stars) included in this study: Aucanquilcha (1) – Ollagüe (2) – Uturuncu (3) transect (Michelfelder et al., 2013); San Pedro (4) – Linzor (5) volcanic chain (SPLVC), including La Poruña scorica cone (6), and Paniri (7), Cerro del León (8) and Toconce (9) volcanoes (Godoy et al., 2014); Putana (10) – Sairecabur (11) – Licancabur (12) transect, including Purico-Chascón Volcanic Complex (13), and Lascar volcano (14). Dotted areas indicate distribution of Altiplano-Puna Volcanic Complex (APVC, thick) and surface projection of the Altiplano-Puna Magma Body (APMB, thin) (after Zandt et al., 2003). Dashed grey areas indicate extend of joint ambient noise-receiver function inversion S-velocity (V_s) models contours, at 15 km b.s.l., for velocities <3.2 km/s (Ward et al., 2014). Thick lined polygon indicates extend of geological map from Fig. 2.

efficiently mixed and at higher proportions with parental mafic magmas and therefore have more leverage on the geochemical composition of the erupted lavas than solid crust. Here we use radiogenic isotopes and geochronological data to map the influence of the APMB. To this end we present new geochronological ($^{40}Ar/^{39}Ar$) and isotopic ($^{87}Sr/^{86}Sr$ and $^{143}Nd/^{144}Nd$) data combined with a compilation of published geochemical data from the NW-SE San Pedro – Linzor volcanic chain (SPLVC) in N. Chile (Fig. 1). This 65 km long linear chain strikes at an angle to the general N-S direction of the Central Andes active front and crosses the western margin of the surficial projection of the upper crustal APMB (Fig. 1).

2. Geological background

Extending from 14°S to 27°, from southern Peru to Central Chile, the modern volcanic arc of the Central Volcanic Zone is built above where the subducting plate is dipping at ~30°; the northern and southern limits are where, respectively, the Nazca and Juan Fernandez and Nazca ridges are currently subducting at shallow angles (de Silva and Francis, 1991; Stern, 2004). For this volcanic arc, four main phases of activity are defined during the eastward migration of the volcanic front (the Andean-Cycle) (e.g. Coira et al., 1982; Scheuber and Giese, 1999; Trumbull et al., 2006): 1) a Jurassic – Upper Cretaceous arc, with effusive products mainly erupted in the Coastal Range in Chile; 2) a Mid-Cretaceous arc of the Longitudinal Valley and Sierra de Moreno in Chile; 3) a Late Cretaceous – Paleogene arc, and after a period of flat-slab subduction, 4) the Miocene – Holocene active volcanic arc with eruptive products mainly located at the Western Cordillera related to steepening (10 to 30°) subduction of the Nazca plate below the South American plate (Coira et al., 1982).

The study region along the arc front and the APVC is characterized in the past 12 M.y. by (Aitcheson and Forrest, 1994) scattered stratovolcanoes along the active arc front and on the Altiplano plateau, (Allmendinger et al., 1997) the eruption of large ignimbrite sheet from several calderas, with repeated eruptions, (de Silva et al., 2006, de Silva and Gosnold, 2007; Salisbury et al., 2011; Kern et al., 2016), and (Arancibia et al., 2006) eruption of young (<100 k.y.) rhyodacitic domes and coulées (de Silva et al., 1994; Watts et al., 1999; Tierney et al., 2016). The ignimbrites are mostly "monotonous intermediates" (sensu Hildreth, 1981) dominantly calc-alkaline, high-K dacites to rhyodacites, with minor rhyolites. Andesitic bands and andesite inclusions in pumices are observed. The dominant volume of ignimbrites is related to large-scale and structurally-controlled collapse calderas (e.g. La Pacana, Guacha, and Pastos Grandes), with significant volumes (>100 km^3) of magma occurrying form "ignimbrite shields" (e.g. Cerro Panizos, the Laguna Colorado shield, and Cerro Purico) (de Silva and Gosnold, 2007; Salisbury et al., 2011). The ignimbrites and domes are typically crystal-rich (>40 vol%) with phenocrysts of plagioclase, quartz, biotite, amphibole, and Fe-Ti oxides with occasional sanidine, along with ubiquitous apatite, titanite, and zircon (Ort et al., 1996; Lindsay et al., 2001; Schmitt et al., 2001; Grocke et al., 2016), showing a strong crustal composition (Lindsay et al., 2001; Schmitt et al., 2001; Kay et al., 2010; Salisbury et al., 2011; Burns et al., 2015; Freymuth et al., 2015; Grocke et al., 2016).

The San Pedro – Linzor volcanic chain (SPLVC) forms a ~65 km long NW-SE trending lineament of stratovolcanoes between 21°53′S 68°23′W and 22°09′S 67°58′W (Figs. 1 and 2). This chain of stratovolcanoes erupted on the NW margin of the APVC and crosses the western border of the APMB (Fig. 1). It includes a series of large and partly complex volcanic edifices (San Pedro – San Pablo volcanic complex, and Paniri, Cerro del León, Toconce, and Linzor volcanoes) consisting of lava, pyroclastic and scoria flows and breccias. Petrographically, lava flows of these volcanoes vary from basaltic-andesite to hornblende-dacite, with pyroxene andesite as the main lithological type. Pyroclastic flows are dacitic, while scoria flows and breccias vary from basaltic-andesite to andesite. (Ramírez and Huete, 1981; Marinovic and Lahsen, 1984; O'Callaghan and Francis, 1986; Lazcano et al., 2012; López et al., 2012; Polanco et al., 2012; Silva et al., 2012; López, 2014; Martínez, 2014; Silva, 2015; Lazcano, 2016). The ~100 ka Chillahuita dome and giant Chao dacitic coulée (Guest and Sanchez, 1969; de Silva et al., 1994; Tierney et al., 2016) are also included in the chain (Fig. 2). Finally, the ~103 ka La Poruña basaltic-andesite scoria cone is the source of a 8 km long lava flow at the far NW end of the SPVC (O'Callaghan and Francis, 1986; Wörner et al., 2000). The SPLVC is underlain mainly by the dacitic Sifon Ignimbrite (8.3 Ma, Salisbury et al., 2011) and ignimbrites and volcaniclastics of the 6.5 to 5.6 Ma Toconce Formation, on older (pre-Neogene) volcanic and volcaniclastic sediments (Ramírez and Huete, 1981; Marinovic and Lahsen, 1984; de Silva, 1989).

3. Analytical methods

3.1. Geochronology

Four of our samples were dated by $^{40}Ar/^{39}Ar$ analyses at the Oregon State University (OSU) Argon Geochronology Laboratory (USA). The samples were crushed in an iron jaw crusher and then sieved. Afterwards 200 mg of the 100–500 μm size-fraction of unaltered groundmass from each sample were hand-picked. Preparation and analyses of samples and standards followed the procedures described in Koppers et al. (2003). Fourteen additional samples were prepared for $^{40}Ar/^{39}Ar$ analyses at the Servicio Nacional de Geología y Minería, Chile (SERNAGEOMIN) on amphibole and unaltered groundmass. Crushing and mineral separation, sample preparation, and analysis were carried out following the procedures and parameters established in Arancibia et al. (2006).

3.2. Geochemistry and isotope analyses.

Thirty-seven samples were crushed in an iron jaw crusher and powdered in agate mills. Geochemical and isotopic analyses were carried out at the GZG (Universität Göttingen, Germany), at the Department of Geological Sciences, University of Cape Town (UCT; South Africa), and at Activation Laboratories Ltda. (Actlabs; Canada). Procedures for X-ray fluorescence (XRF; major and trace element concentrations) and thermal ionization mass spectrometry (TIMS; $^{87}Sr/^{86}Sr$ and $^{143}Nd/^{144}Nd$ ratios) analyses at GZG are described in Godoy et al. (2014). Two-sigma analytical errors were <2% for XRF, and <0.004% for $^{87}Sr/^{86}Sr$ and $^{143}Nd/^{144}Nd$ ratios. At UCT samples were analyzed by XRF and Inductively Coupled Plasma – Mass Spectrometry (ICP-MS) for major and trace elements, following the procedures, standards and parameters detailed in Frimmel et al. (2001). $^{87}Sr/^{86}Sr$ and $^{143}Nd/^{144}Nd$ ratios were measured at UCT by NuPlasma HR multi collector-ICP-MS (MC-ICP-MS). Sample preparation and equipment conditions for these analyses are detailed in Harris et al. (2015). Analytical errors (2 S.D.) were <2% for XRF, <3% for ICP-MS and <0.003% for $^{87}Sr/^{86}Sr$ and $^{143}Nd/^{144}Nd$ ratios. At Actlabs, inductively coupled plasma-optical emission spectrometry (ICP-OES), ICP-MS, and TIMS were utilized for major oxides, trace elements, and $^{87}Sr/^{86}Sr$ and $^{143}Nd/^{144}Nd$ analyses, respectively. For ICP-OES and ICP-MS, samples were mixed with a flux of lithium metaborate and lithium tetraborate and fused in an induction furnace. The melt was immediately poured into a solution of 5% nitric acid containing an internal standard, and mixed continuously until completely dissolved (~30 min). Analytical errors are <2% for each type of analyses. For TIMS, Rb and Sr, and Sm and Nd were separated by extraction chromatography. The analyses were performed on a Thermo Triton thermal ionization multi-collector mass spectrometer. Errors for $^{87}Sr/^{86}Sr$ and $^{143}Nd/^{144}Nd$ ratios were <0.004%. For these analyses more information about analytical procedure, equipment and uncertainties are available at: http://www.actlabs.com. Our data are compiled in Table 1 where the different laboratories and methods are identified for each sample.

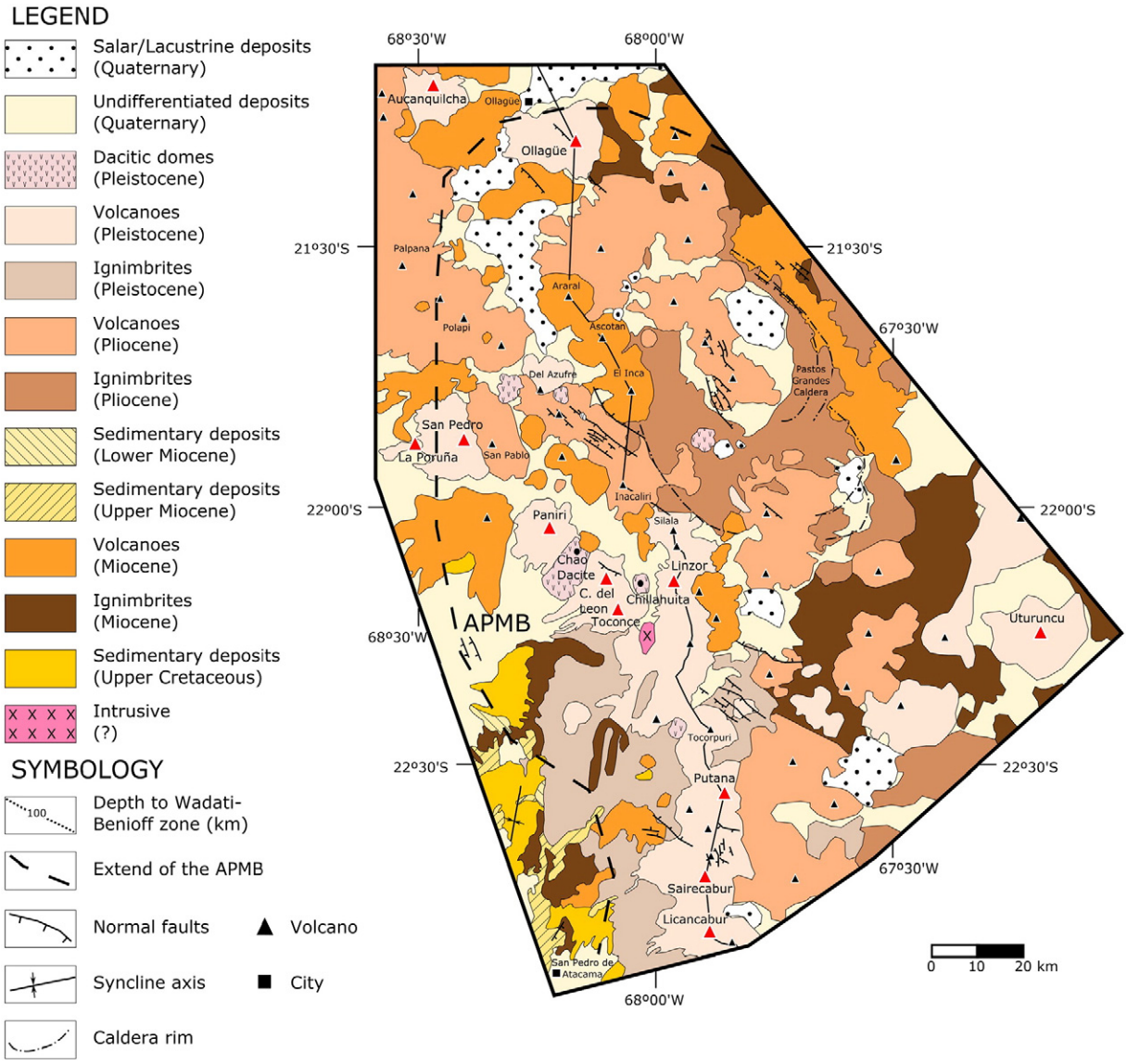

Fig. 2. Geological map of a section of the Central Volcanic Zone of the Andes from Aucanquilcha to Licancabur volcanoes (after Tibaldi et al., 2009), with ignimbrite distribution after Salisbury et al. (2011), and geology of Uturuncu volcano after Sparks et al. (2008). Extend of Altiplano-Puna Magma Body (APMB) after Zandt et al. (2003). Volcanoes included in this study on red triangles.

4. Results

4.1. Main petrological and geochemical features of the San Pedro-Linzor volcanic chain.

Although some volcanoes from the SPLVC show hydrothermal alteration at their cores and flanks (e.g. Toconce, Cerro del León), analyzed samples were obtained from largely unaltered, dense lava flows. This selection resulted in a bias towards younger lavas. Lavas classify as basaltic-andesite to rhyolite with predominance of dacitic compositions (Fig. 3; Table 1). Plagioclase and ortho- and clinopyroxene are the main phenocrysts in a matrix consisting of 60 to 75 vol% of plagioclase and pyroxene microlites, and glass (Fig. 4). At Paniri and San Pedro volcanoes, andesites have rare olivine phenocrysts (<5 vol%) with skeletal texture (Fig. 4), while at Toconce and Cerro del León olivine is even scarcer (<2 vol%). Amphibole and biotite are rare, with amphibole showing disequilibrium textures at the rims. Moreover, resorbed quartz phenocrysts have been observed in Linzor dacite lavas (Fig. 4).

4.2. $^{40}Ar/^{39}Ar$ ages

$^{40}Ar/^{39}Ar$ results are presented in Tables 2 and 3. Ages were obtained by using the Isoplot excel spreadsheet (Ludwig, 2012). Plateau ages were defined as containing >70% of the total ^{39}Ar released. Age plateaus and inverse isochron ages are in concordance at the 95% confidence level (Tables 2 and 3). Age spectra and inverse isochron diagrams of representative samples are shown in Figs. 5 and 6. Ages obtained on amphibole mineral separates show a larger error than those obtained from unaltered groundmass (Fig. 5; Table 3). Sample PAE-15 shows no age plateau and only three steps were used to calculate the inverse isochron age (Fig. 5), the age obtained for this sample is therefore not reliable. The age obtained for sample PAE-09 was calculated by combining data from two analyses, both showing concordant isochron and spectra ages (Fig. 6; Table 3).

Paniri volcano shows the oldest (1.390 ± 0.290 Ma), and the youngest (150 ± 6 ka) age for the volcanic chain (Fig. 7). For Cerro del Leon, $^{40}Ar/^{39}Ar$ dating indicates flows with ages of 1.054 ± 0.011 Ma to 275

Table 1
SiO_2, Na_2O, K_2O, Sr, Nd, $^{87}Sr/^{86}Sr$, and $^{143}Nd/^{144}Nd$ content of analyzed samples from San Pedro – Linzor volcanic chain.

Volcano	Sample	Latitude (S)	Longitude (W)	SiO_2[a] (wt%)	Na_2O[a] (wt%)	K_2O[a] (wt%)	Sr (ppm)	Nd (ppm)	$^{87}Sr/^{86}Sr$	Error (2S.D.) (10^{-6})	$^{143}Nd/^{144}Nd$	Error (2.S.D.) (10^{-6})
La Poruña	SP1[b]	21° 53′ 14″	68° 29′ 58″	56.70	3.66	1.72	578	19	0.706630	–	0.512378	–
	POR-14-01[f]	21° 53′ 27″	68° 30′ 39″	56.21	3.72	1.70	608	–	0.706640	8	0.512393	12
	POR-15-02[f]	21° 53′ 29	68° 29′ 47″	57.80	3.72	1.83	584	–	0.706265	11	0.512427	11
	POR-15-03[f]	21° 53′ 32″	68° 29′ 58″	57.29	3.63	1.76	575	–	0.706353	13	0.512421	13
	POR-15-04[f]	21° 53′ 35″	68° 30′ 19″	57.07	3.57	1.77	569	–	0.706272	12	0.512450	12
	POR-15-05[f]	21° 55′ 32″	68° 34′ 2″	59.34	3.91	2.10	590	–	0.706184	10	0.512437	11
San Pedro	SPP-98-54[b]	21° 52′ 12″	68° 29′ 52″	63.60	4.88	2.72	518	14	0.706660	–	0.512351	–
	SPP-98-56[b]	21° 49′ 24″	68° 27′ 50″	64.10	4.32	2.86	512	22	0.705710	–	0.512346	–
	BG-SPL-004[e]	21° 54 ‘22″	68° 30′ 3″	58.50	3.67	1.91	523	20	0.706149	4	–	–
	BG-SPL-010[e]	21° 50′ 1″	68° 30′ 1″	57.70	3.66	1.67	610	20	0.706705	5	–	–
	BG-SPL-015[c]	21° 53′ 25″	68° 29′ 33″	57.40	3.69	1.77	508	17	0.706306	9	0.512404	3
	SPSP-14-01[f]	21° 49′ 55″	68° 29′ 48″	62.41	4.37	2.67	584	–	0.706683	1	0.512392	11
	SPSP-14-02[f]	21° 56′ 3″	68° 30′ 36″	63.20	4.05	3.16	489	–	0.706414	1	0.512384	12
Paniri	BG-SPL-019A[c]	22° 1′ 28″	68° 16′ 6″	68.80	3.86	3.84	365	29	0.707143	3	0.512347	5
	BG-SPL-022[c]	22° 2′ 48″	68° 17′ 4″	56.50	3.47	1.52	663	17	0.706676	6	0.512279	6
	BG-SPL-023A[c]	21° 59′ 05″	68° 14′ 45″	61.60	3.50	2.71	441	25	0.707212	3	0.512338	3
	BG-SPL-044A[c]	22° 8′ 24″	68° 16′ 26″	65.00	3.45	3.61	407	28	0.707253	3	0.512268	4
	PANI-12-02[f]	22° 0′ 55″	68° 15′ 11″	65.40	3.97	3.22	432	23	0.70723	15	0.512352	10
	PANI-12-07[f]	22° 3′ 48″	68° 11′ 46″	69.70	3.81	3.79	359	25	0.707977	12	0.512317	10
	PANI-12-08v	22° 4′ 16″	68° 11′ 41″	65.80	3.81	3.03	439	24	0.707577	12	0.512326	7
	PANI-12-10[f]	22° 2′ 49″	68° 15′ 14″	67.40	3.93	3.52	421	25	0.706909	13	0.512351	10
	PANI-12-14[f]	22° 7′ 49″	68° 0′ 11″	66.10	3.44	3.64	393	26	0.707294	13	0.512366	10
	PANI-12-15[f]	22° 7′ 32″	68° 16′ 4″	64.80	3.64	3.39	431	25	0.707318	13	0.512334	9
	M28[g]	22° 6′ 10″	68° 18′ 12″	64.40	3.45	3.32	417	28	0.707333	4	0.512339	6
Cerro del Leon	BG-SPL-040[c]	22° 13′ 59″	68° 14′ 45″	60.90	3.16	3.02	458	–	0.707875	3	0.512237	4
	LEO-10-01[c]	22° 9′ 30″	68° 8′ 01″	63.20	3.39	3.17	408	28	0.707821	3	0.512245	6
	LEO-10-02[e]	22° 9′ 32″	68° 8′ 01″	62.60	3.39	2.95	419	28	0.707811	4	–	–
	LEO-10-07[e]	22° 13′ 46″	68° 16′ 52″	60.50	3.46	2.60	464	25	0.707899	4	–	–
	LEO-12-01[f]	22° 6′ 27″	68° 7′ 40″	69.40	4.51	4.29	278	31	0.708045	15	0.512322	8
	LEO-12-03[f]	22° 5′ 54″	68° 7′ 42″	68.70	4.45	4.18	319	33	0.708036	12	0.512330	8
	LEO-12-04[f]	22° 5′ 24″	68° 7′ 44″	62.80	3.77	2.94	435	29	0.70794	10	0.512313	9
	LEO-12-07[f]	22° 7′ 20″	68° 7′ 2″	65.20	2.79	3.46	348	28	0.709573	9	0.512276	9
	LEO-12-09[f]	22° 6′ 57″	68° 6′ 38″	67.50	4.02	3.80	319	28	0.70788	11	0.512333	8
	LEO-12-C2[f]	22° 8′ 41″	68° 4′ 54″	65.70	3.33	3.46	350	24	0.708334	9	0.512267	9
	M25b[g]	22° 11′ 37″	68° 10′ 58″	63.70	3.03	3.32	386	26	0.707765	3	0.512302	11
Toconce	BG-SPL-048[c]	22° 10′ 1″	68° 3′ 20″	58.80	3.07	2.11	503	24	0.707693	4	0.512296	10
	TOC-10-02[e]	22° 13′ 17″	68° 5′ 42″	63.50	3.35	3.10	391	27	0.708347	3	–	–
	TOC-10-03[c]	22° 12′ 49″	68° 5′ 14″	69.40	3.23	4.42	267	28	0.709346	6	0.512269	20
	TOC-10-04[c]	22° 12′ 49″	68° 5′ 06″	64.70	3.21	3.47	338	31	0.708998	1	0.512242	9
	TOC-10-08[e]	22° 14′ 15″	68° 5′ 24″	66.80	3.06	3.83	335	30	0.708527	1	–	–
	TOC-12-01[f]	22° 9′ 3″	68° 4′ 10″	68.80	3.25	4.01	292	24	0.708836	12	0.512244	9
	TOC-12-02[f]	22° 9′ 8″	68° 3′ 57″	62.90	3.33	2.98	430	26	0.708026	14	0.512293	8
	TOC-12-04[f]	22° 10′ 42″	68° 4′ 2″	65.90	3.67	3.24	418	26	0.707848	12	0.512296	11
	TOC-12-05[f]	22° 10′ 42″	68° 4′ 2″	66.40	3.65	3.43	390	26	0.707844	14	0.512285	11
	TOC-12-10[f]	22° 15′ 8″	68° 12′ 54″	67.30	3.23	4.27	272	27	0.708786	12	0.512286	12
	TOC-15-01[f]	22° 11′ 48″	68° 3′ 50″	65.34	3.99	3.16	372	–	0.707601	1	0.512310	10
	M21[g]	22° 14′ 58″	68° 7′ 49″	67.60	2.81	4.45	235	29.5	0.708812	3	0.512281	3
Chao Dacite	88054[d]	–	–	67.90	3.25	3.81	335	–	0.70806	–	0.51224	–
Chillahuita	84058[d]	–	–	68.80	3.42	3.66	325	–	0.70805	–	0.51224	–

[a] Recalculated 100% water free.
[b] Data from Mamani et al. (2010).
[c] Data from Godoy et al. (2014).
[d] Data from de Silva et al. (1994).
[e] Analysis at University of Göttingen (Germany).
[f] Analysis at University of Cape Town (South Africa).
[g] Analysis at ActLabs (Canada).

± 7 ka, while Toconce volcano shows flows ranging in age from 1.294 ± 0.080 Ma to 891 ± 33 ka (Fig. 7).

4.3. $^{87}Sr/^{86}Sr$ and $^{143}Nd/^{144}Nd$ isotope ratios

Published and new $^{87}Sr/^{86}Sr$ and $^{143}Nd/^{144}Nd$ data, together with SiO_2 (wt%), and Sr and Nd (ppm) contents of lavas erupted in the SPLVC are presented in Table 1 including data from La Poruña scoria cone and Chao Dacite and Chillahuita domes. $^{87}Sr/^{86}Sr$ ratios between 0.706184 and 0.706640, and $^{143}Nd/^{144}Nd$ ratios between 0.512378 and 0.512450 have been obtained for La Poruña lavas (Mamani et al., 2010; Table 1), while San Pedro volcano shows values from 0.705710 to 0.706705, and from 0.512346 to 0.512404, respectively (compiled from literature data in Mamani et al., 2010; Table 1). Paniri lavas have $^{87}Sr/^{86}Sr$ between 0.706676 and 0.707977, which are significantly higher than values for San Pedro and La Poruña, while the $^{143}Nd/^{144}Nd$ ratios are lower (0.512268 to 0.512366). $^{87}Sr/^{86}Sr$ isotope ratios of Cerro del Leon lavas vary from 0.707811 to 0.709573, while $^{87}Sr/^{86}Sr$ isotope ratios of Toconce range between 0.707693 and 0.709346. $^{143}Nd/^{144}Nd$ ratios for Cerro del Leon vary between 0.512237 and 0.512333, and for Toconce vary from 0.512242 and 0.512310. Both volcanoes exhibit Sr isotope ratios higher than, and

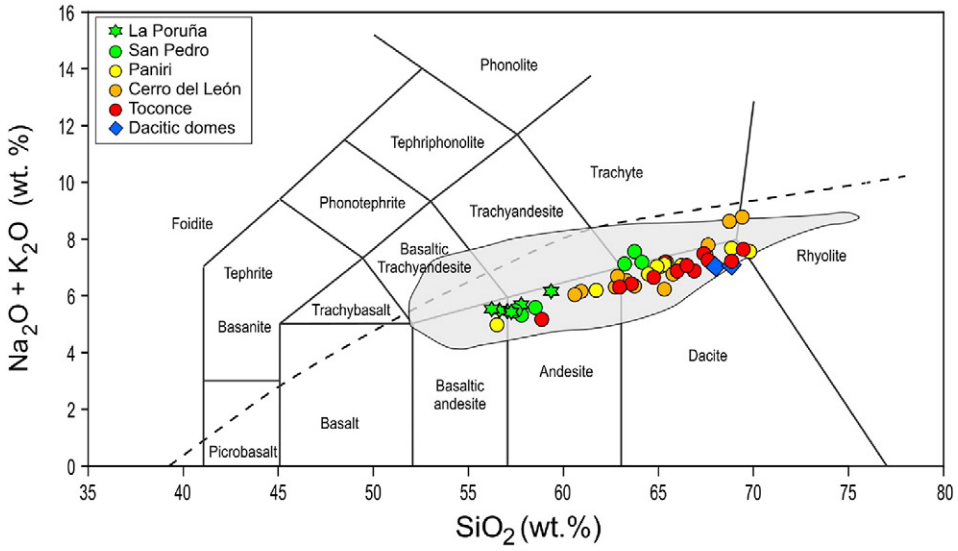

Fig. 3. Total-Alkali vs. Silica (TAS) diagram (after Le Maitre, 1984) for analyzed lavas of SPLVC, and Chao Dacite and Chillahuita dacitic domes (Table 1). Lava samples show a well-defined sub-alkaline trend, varying from basaltic-andesite to rhyolitic, with some trachytic composition. Field represents the composition of Central Andes lavas (after Mamani et al., 2010). Segmented line represents subdivision of alkaline and subalkaline lavas (after Irvine and Baragar, 1971).

overlapping, those obtained by de Silva et al. (1994) for the Chao Dacite and Chillahuita dacitic domes (~0.7081) (Table 1).

5. Discussion

5.1. Age relations

New $^{40}Ar/^{39}Ar$ ages (Tables 2 and 3) and published age data (Table 4) show an increase in age for the SPLVC from the NW towards the SE in parallel to the increase in Sr-isotope ratios (Fig. 7). At the SPLVC the oldest lavas correspond to a series of flows at the base of Paniri volcano (1.390 ± 0.290 Ma), at the base (1.054 ± 0.011 Ma) and the southern flank (0.913 ± 0.080 Ma) of Cerro del Leon volcano, and at the lower southern flanks of Toconce volcano (>0.9 Ma). This suggests that the initial construction of the volcanic edifices along the chain was more or less contemporaneous, between 0.9 and 1.5 Ma. After that, the younger parts of the edifices formed progressively north-westwards. Thus, the youngest lavas dated for the volcanic chain correspond to Paniri volcano, with 164 ± 3 and 150 ± 6 ka, respectively, and at Cerro del Leon, with 275 ± 7 ka. For San Pedro volcano, historical activity and fumarole emissions have been reported (Global Volcanism Program, 2013). O'Callaghan and Francis (1986) suggested that this volcano is younger than San Pablo, which pre-dated the last glacial episode. Moreover, a $^{40}Ar/^{39}Ar$ age of 107 ± 12 ka was obtained for the southern lava flow of the volcano (Delunel et al., 2016). Thus, a Pre-Holocene to Recent age is proposed for this volcano (Fig. 7). On the other hand, the eruption

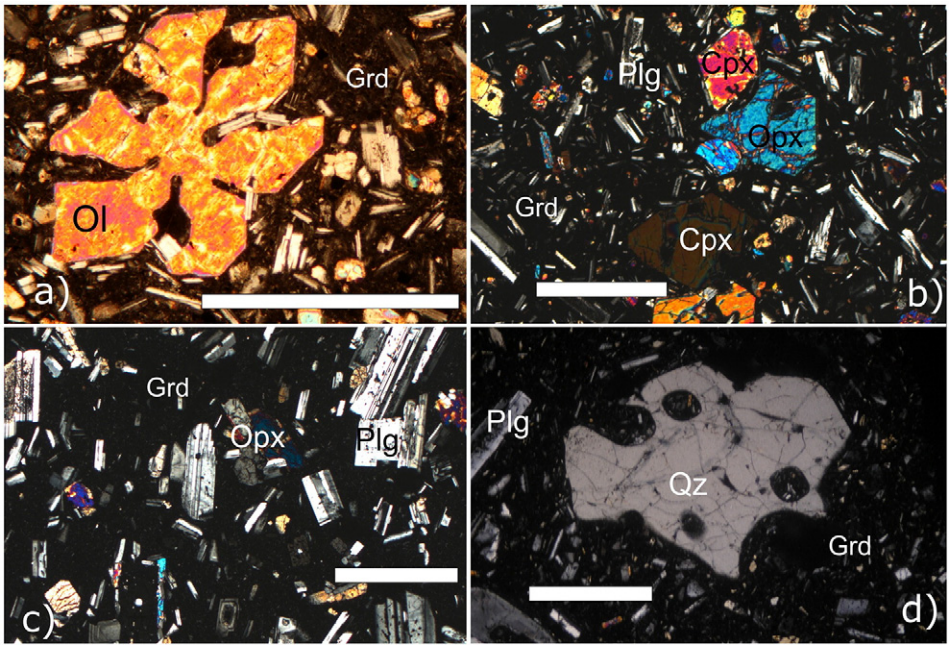

Fig. 4. Photomicrographs showing typical textures of lavas from the SPLVC. a) Skeletal olivine (Ol) in a plagioclase + glass groundmass (Grd) from Paniri volcano (sample BG-SPL-022, 10×). b) Clinopyroxene (Cpx), orthopyroxene (Opx), and plagioclase (Plg) in plagioclase + glass groundmass (Grd) from San Pedro volcano (sample BG-SPL-015, 2×). c) Orthopyroxene (Opx) and plagioclase (Plg) in a glassy groundmass (Grd) from Toconce volcano (sample TOC-10-04, 2×). d) Embayed quartz (Qz), and plagioclase (Plg), in a plagioclase + glass groundmass (Grd), lava from Linzor volcano (BG-SPL-030, 2×). All bars indicate 1 mm length.

Table 2
$^{40}Ar/^{39}Ar$ from incremental heating analyzed lava samples at OSU Argon Geochronology Lab (USA).

Sample	Latitude (S)	Longitude (W)	Sample description	Phase[b]	Age spectrum					Inverse isochron analyses					
					Age (Ma)	Error (2σ)	^{39}Ar (%)	n[c]	[a]	Age (Ma)	Error (2σ)	n[c]	$^{40}Ar/^{36}Ar$ intercept	Error (2σ)	[a]
BG-SPL-022	22° 2′ 48″	68° 17′ 4″	Western flank of Paniri. andesitic flow	gm	**0.402**	**0.460**	95.8	9/11	0.03	0.380	0.560	9/11	297.0	13.0	0.03
BG-SPL-040	22° 13′ 59″	68° 14′ 45″	S flank of C. del Leon, dacitic flow	gm	**0.913**	**0.080**	93.8	10/12	0.24	0.890	0.330	10/12	294.9	4.2	0.26
TOC-10-04	22° 12′ 49″	68° 5′ 6″	Upper S flank of Toconce, dacitic flow	gm	**0.891**	**0.033**	100.0	12/12	0.08	0.891	0.037	12/12	295.5	1.6	0.09
TOC-10-09	22° 14′ 55″	68° 5′ 51″	S flank of Toconce, andesitic flow	gm	**1.294**	**0.080**	100.0	13/13	0.19	1.240	0.360	13/13	296.0	2.7	0.20

[a] MSWD – mean square of weighted deviates. Preferred ages are in bold.
[b] Abbreviation: gm – groundmass.
[c] Number of data points used in plateau and isochron calculations; each step heating represents one data point.

of the mafic lava in the area at La Poruña scoria cone, at the NW end of the chain, occurred at ~100 ka (^{3}He exposure age; Wörner et al., 2000) contemporaneous with the formation of the silicic domes (Chao and Chillahuita) in the center and the SE end of the chain (ages in Tierney et al., 2016; Fig. 7).

In summary, published K/Ar, ^{3}He, as well as published and new $^{40}Ar/^{39}Ar$ geochronological data indicate that the SPLVC evolved during the last 2 Ma with activity continuing into the Holocene at San Pedro, Paniri and possibly Cerro de Leon volcano, based on morphological observations. These are consistent with the age data, suggesting a younging of activity, in the last 1 M.y., along the chain from SE to NW, i.e. from Toconce to San Pedro (Fig. 7). Contemporaneous eruption of basaltic-andesite and siliceous magmas, however, occurred between 80 and 110 ka with La Poruña scoria cone, and Chao and Chillahuita domes along the entire chain.

Within this relatively short time-window (1.3 Ma) Sr-isotopes show no correlation with age (Fig. 8). This is different on a local scale for the evolution of individual stratovolcanoes, e.g. the Purico – Chascon volcanic complex (Burns et al., 2015) and Aucanquilcha Volcanic Cluster (Grunder et al., 2006; Klemetti and Grunder, 2008; Walker, 2011; Walker et al., 2013), where decreasing on Sr-isotopes indicate waning of the magmatic systems (Fig. 1). Moreover, temporal shifts in isotopic composition of magmas observed on the larger temporal (>10 Ma) and spatial (>100 km) scale in the Central Andes in general (e.g. Mamani et al., 2010 and reference therein) are related to crustal thickening (McMillan et al., 1993; Haschke, 2002; Haschke et al., 2006) and composition (Wörner et al., 1992; Mamani et al., 2010). Thus, in contrast to the general evolution across the Central Andes, isotopic shifts at the SPLVC, and the other volcanoes selected here for comparison (e. g. Uturuncu, Licancabur, Aucanquilcha, Ollagüe, and the active Lascar volcano, Gardeweg et al., 2011), in the last 2 M.y. cannot be related to (1) differences in the composition of the underlying crust, (2) increased assimilation with time in a thickening crust or (3) during thermal evolution of a MASH system.

5.2. Sr- and Nd-isotope variation by different degree of crustal assimilation?

Fig. 9 shows $^{143}Nd/^{144}Nd$ vs. $^{87}Sr/^{86}Sr$ isotope compositions in lavas from along the SPLVC, together with selected literature data from volcanoes at different position with respect to the border of the APMB (Feeley and Davidson, 1994; Matthews et al., 1994; Figueroa et al., 2009; Mamani et al., 2010; Walker, 2011; Michelfelder et al., 2013). The NW to SE isotopic variation between Aucanquilcha, Ollagüe, and Uturuncu volcanoes follow the same isotopic trend as that from S to N from Lascar volcano to the Putana-Sairecabur-Licancabur volcanic chain (Fig. 1) and along the NE-SW- trending SPLVC. The most "crustal" apex of the trends corresponds to Uturuncu volcano (Fig. 9) which also lies within the central part of the APMB with lowest S-wave seismic velocities of <2.1 km/s (Ward et al., 2014; Fig. 1). Less crustal isotopic signatures then correlate with higher seismic velocities as the transects are crossing the margin of the partially molten APMB zone (Fig. 9).

As a negative linear correlation exists between Sr and Nd isotopic systems, increasing Sr-ratios while Nd ratios decrease, we focus on Sr-isotope characteristics of the SPLVC, related to the degree of crustal contamination. In this case, the SPLVC shows a southeastward increase of $^{87}Sr/^{86}Sr$ with decreasing Sr concentration (Fig. 10a). This observation is typical for many but not all composite cones in the Andean CVZ (Davidson et al., 1990) and can be interpreted to reflect increasing

Table 3
$^{40}Ar/^{39}Ar$ from incremental heating analyzed lava samples at SERNAGEOMIN (Chile).

Sample	Latitude (S)	Longitude (W)	Sample description	Phase[b]	Age spectrum					Inverse isochron analyses					
					Age (Ma)	Error (2σ)	^{39}Ar (%)	n[c]	[a]	Age (Ma)	Error (2σ)	n[c]	$^{40}Ar/^{36}Ar$ intercept	Error (2σ)	[a]
PAE-02	22° 2′ 47″	68° 12′ 35″	N flank of Paniri, dacitic flow	amph	**0.264**	**0.099**	100.0	8/8	0.67	0.240	0.160	7/8	296.9	4.4	0.71
PAE-03	22° 2′ 50″	68° 12′ 29″	N flank of Paniri, dacitic flow	gm	**0.325**	**0.008**	100.0	8/8	0.45	0.323	0.012	8/8	295.8	3.0	0.50
PAE-08	22° 6′ 13″	68° 17′ 49″	SW flank of Paniri, andesitic flow	amph	**0.150**	**0.006**	100.0	8/8	1.40	0.151	0.007	7/8	292.5	6.6	1.18
PAE-09[0]	22° 0′ 0″	68° 14′ 8″	N flank of Paniri, dacitic flow	amph	–	–	–	–	–	**1.390**	**0.290**	13/15	297.0	4.6	0.49
PAE-09[1]	22° 0′ 0″	68° 14′ 8″	N flank of Paniri, dacitic flow	amph	0.980	0.360	100.0	8/8	0.97	0.970	0.460	8/8	297.0	11.0	1.12
PAE-09[2]	22° 0′ 0″	68° 14′ 8″	N flank of Paniri, dacitic flow	amph	1.420	0.300	100.0	7/7	0.72	1.370	0.340	7/7	297.6	5.0	0.75
PAE-15	22° 6′ 48″	68° 7′ 12″	W flank of C. del Leon, dacitic flow	gm	–	–	–	–	–	**1.137**	**0.051**[d]	3/8	295.7	8.9	0.17
PAE-16	22° 3′ 42″	68° 6′ 42″	NE flank of C. del Leon, trachy-dacitic flow	gm	**1.054**	**0.011**	76.7	5/8	0.64	1.037	0.032	7/8	297.4	3.5	0.70
PAE-25	22° 3′ 44″	68° 15′ 31″	E flank of Paniri, trachy-dacitic flow	gm	**0.164**	**0.003**	100.0	8/8	0.76	0.163	0.003	8/8	295.6	4.1	0.90
PAE-36	22° 11′ 49″	68° 8′ 33″	S flank of C. del Leon, andesitic flow	gm	**0.367**	**0.018**	82.5	3/8	0.54	0.334	0.055	8/8	297.1	2.4	0.50
PAE-37	22° 10′ 0″	68° 7′ 2″	SW flank of C. del Leon, andesitic flow	gm	**0.664**	**0.012**	93.8	7/8	0.16	0.687	0.019	8/8	292.5	1.7	1.7
PAE-42	22° 14′ 37″	68° 7′ 30″	SW flank of Toconce, dacitic flow	gm	**0.959**	**0.005**	100.0	8/8	0.68	0.960	0.005	8/8	294.5	1.7	0.55
PAE-43	22° 7′ 55″	68° 15′ 16″	S flank of Paniri, andesitic flow	amph	**0.625**	**0.093**	100.0	8/8	0.24	0.610	0.110	8/8	298.1	6.4	0.16
PAE-44	22° 11′ 28″	68° 10′ 55″	SW flank of C. del Leon, andesitic flow	gm	**0.628**	**0.007**	97.9	7/8	0.23	0.623	0.008	8/8	298.5	2.0	0.39
PAE-48	22° 9′ 31″	68° 4′ 55″	SE flank of C. del Leon, dacitic flow	gm	0.275	0.007	100.0	8/8	0.05	**0.275**	**0.008**	8/8	295.3	2.1	0.05
PAE-55	22° 3′ 45″	68° 11′ 24″	E flank of Paniri, dacitic flow	amph	**0.640**	**0.140**	97.2	5/7	0.06	0.650	0.200	5/7	291.0	28.0	0.05

PAE-090 as result of combined analyses of PAR-091 and PAE-092.
[a] MSWD - mean square of weighted deviates. Preferred ages are in bold.
[b] Abbreviation: gm – groundmass.
[c] Number of data points used in plateau and isochron calculations; each step heating represents one data point.
[d] Not reliable, see text for discussion.

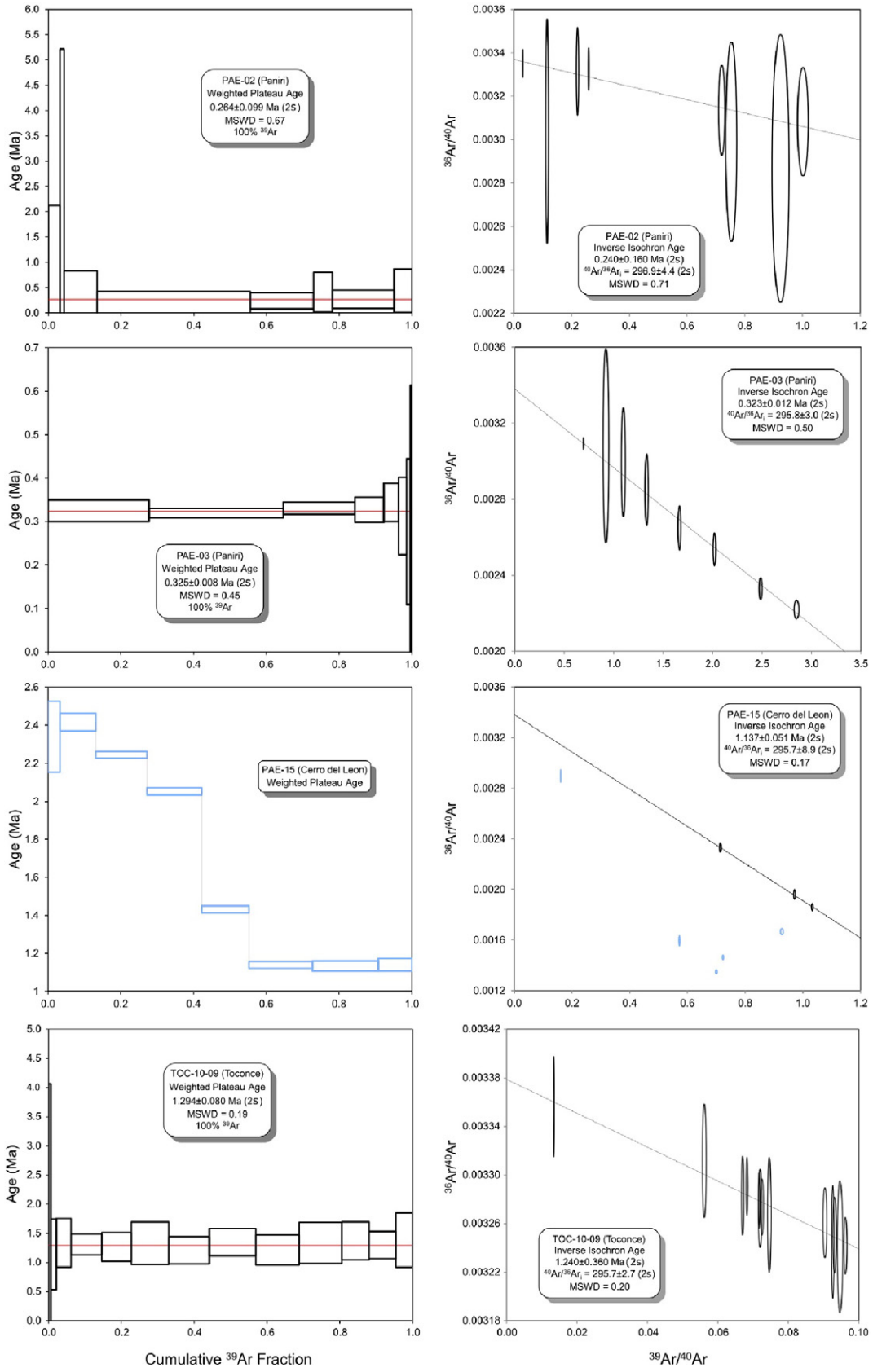

Fig. 5. Age spectra and inverse isochron diagrams for representative samples of dated amphibole (PAE-02) and groundmass (PAE-03, PAE-15 and TOC-10-09). Age diagrams for sample PAE-15 shows no plateau and thus the age from this sample is not reliable. Box heights are 2σ error. Analytical error ellipses in isochron diagrams and initial $^{40}Ar/^{39}Ar$ ($^{40}Ar/^{39}Ar_i$) are at the 2σ level. Light blue data indicate rejected analyses. MSWD = mean standard weighted deviates.

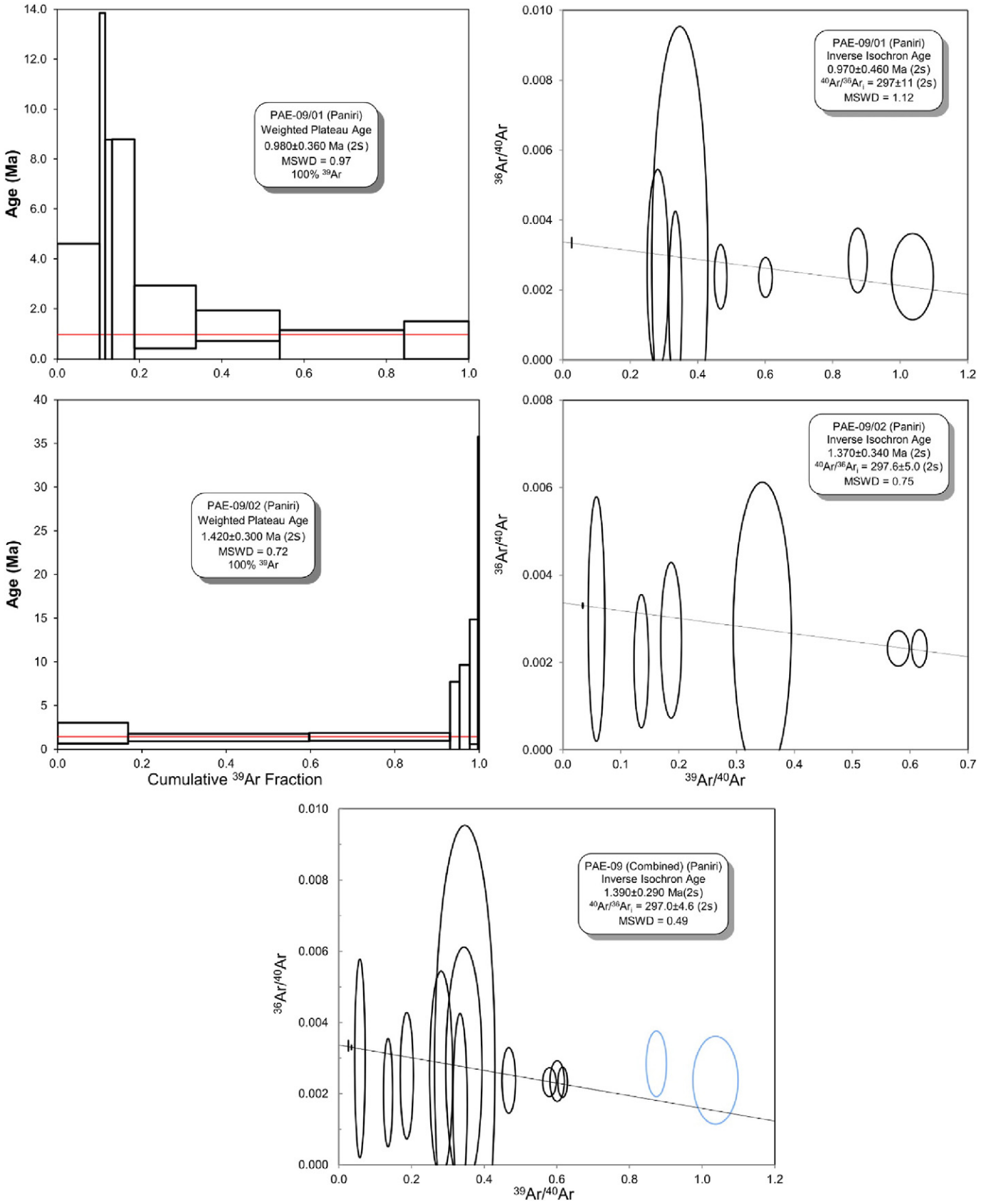

Fig. 6. Age spectra and inverse isochron diagram of two analyses for sample PAE-09 (amphibole). Combined isochron diagram for sample PAE-09 is also shown. Box heights are 2σ error (2 s). Analytical error ellipses in isochron diagrams and initial $^{40}Ar/^{39}Ar$ ($^{40}Ar/^{39}Ar_i$) are at the 2σ level. Light blue data indicate rejected analyses. MSWD = mean standard weighted deviates.

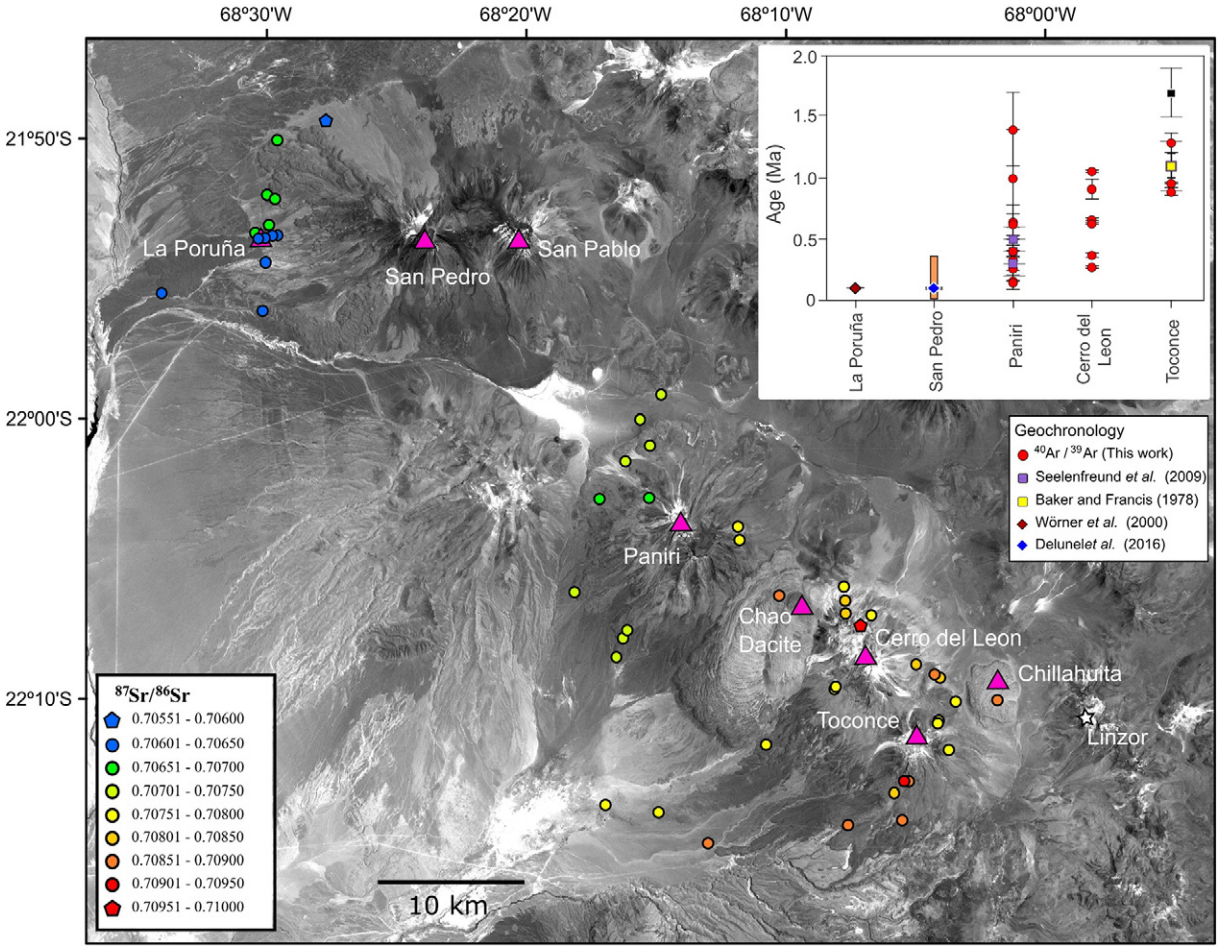

Fig. 7. Satellite image of the SPLVC showing the spatial distribution of $^{87}Sr/^{86}Sr$ isotopic ratios presented on Table 1. Sr-isotope ratios decrease from SE (Toconce volcano) to NW (San Pedro volcano). Inset shows distribution of ages, with errors (2σ). Bar for ages at San Pedro after O'Callaghan and Francis (1986).

proportions of assimilated crustal rocks in magmas together with higher degrees of low-pressure differentiation. As volcanoes of the SPLVC are located entirely in the Antofalla crustal domain (sensu Mamani et al., 2010) parental magmas that ascend from the lower crust should have similar isotopic characteristics (Godoy et al., 2014). Models for further evolution of these basaltic andesite parental magmas involve two fundamentally different, although not mutually exclusive processes of interaction between parental magmas and crustal rocks: (Aitcheson and Forrest, 1994) Assimilation of shallow crustal material during magmatic differentiation mainly by fractional crystallization (the "classic" AFC process, e.g. Davidson et al., 1990; Feeley and Davidson, 1994; Caffe et al., 2002), and (Allmendinger et al., 1997) wholesale mixing between "mashed" parental magmas and crustal melts that may either be derived from melting at deep or shallow crustal levels (e.g. Blum-Oeste and Wörner, 2016). Godoy et al. (2014) have pointed out that magmas erupted along the SPLVC do not have heavy rare earth element-depleted trace element patterns that would be indicative of magma evolution under high pressure (i.e. involving garnet as a residual phase), even though the crust was undoubtedly thick (>60 km) when these lavas were erupted. HREE-depleted patterns, however, do occur in many CVZ lavas erupted (<10 Ma) after the last main phase of crustal thickening of the Central Andes (Mamani et al., 2010). As argued by Godoy et al. (2014), the absence of a deep-crustal geochemical signature for lavas from SPLVC suggests that magma genesis is dominated by shallow assimilation of crustal melts that are derived from the APMB. Thus, lavas erupted at this volcanic chain evolved and assimilated crustal material at shallow levels (Godoy et al., 2014; Martínez, 2014).

Taking into account considerations from other petrologic studies of Central Andes volcanism (e.g. Davidson et al., 1990; Caffe et al., 2002; Kay et al., 2010), simple AFC models (DePaolo, 1981) were used to

Table 4
Published ^{3}He, K/Ar and $^{40}Ar/^{39}Ar$ ages for San Pedro – Linzor volcanic chain.

Sample	Latitude (S)	Longitude (W)	Age (Ma)	error (2σ)	Method	Observations	Reference
POR-02	21° 53′ 5″	68° 30′ 0″	0.103	0.001	^{3}He	Lava flow from La Poruña	Wörner et al. (2000)
SP12–02A	21° 56′ 2″	68° 30′ 36″	0.107	0.012	$^{40}Ar/^{39}Ar$	Lava flow from the SW dome from San Pedro volcano	Delunel et al. (2016)
ZZ-06	22° 12′ 53″	68° 2′ 26″	1.70	0.20	K/Ar	Outcrop on slope of the Toconce volcano	Seelenfreund et al. (2009)
ZZ-11	22° 12′ 54″	68° 2′ 17″	1.10	0.20	K/Ar	Outcrop on slope of the Toconce volcano	Seelenfreund et al. (2009)
ZZ-27a	22° 8′ 30″	68° 16′ 3″	0.50	0.10	K/Ar	Andesitic flow of the ower slope of the Paniri volcano	Seelenfreund et al. (2009)
ZZ-42	22° 5′ 19″	68° 11′ 48″	0.30	0.10	K/Ar	Andesitic flow at the upper slope of the Paniri volcano	Seelenfreund et al. (2009)
ZZ-46	22° 8′ 30″	68° 16′ 3″	0.40	0.10	K/Ar	Andesitic flow of the ower slope of the Paniri volcano	Seelenfreund et al. (2009)
A88-15	22° 15′ 15″	68° 9′ 15″	1.10	0.10	K/Ar	Southern dacitic flow from Toconce volcano	Baker and Francis (1978)

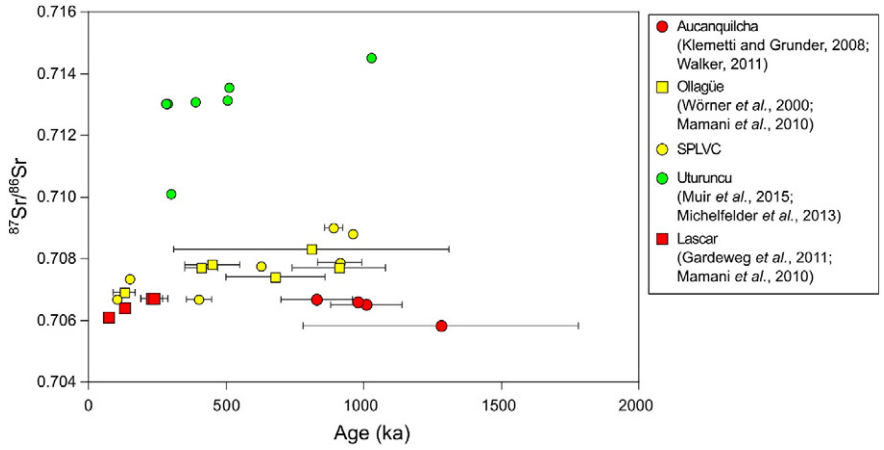

Fig. 8. $^{87}Sr/^{86}Sr$ vs. Age (ka) diagram showing the absence of a clear relationship between the Sr isotope composition and age. For SPLVC isotopic data from samples SPSP-14-02 (San Pedro), M28 (Paniri), M25 (Cerro del Leon), and M21 (Toconce) (Table 1) correspond to geochronological analyses SP12-02A (Delunel et al., 2016), and PAE-08, PAE44 and PAE 42 (Table 3), respectively. Bars indicate 2σ error.

simulate the composition of SPLVC lavas, constraining the amount of crustal material using Eq. (5) from the RAFT model by Aitcheson and Forrest (1994). As an initial composition, we consider the basaltic-andesite (BA) end-member proposed as parent magmas of the Central Andes (Blum-Oeste and Wörner, 2016). Thus, a sample from Lascar volcano (Table 5) was selected. This sample shows low Sr-isotope ratio (~0.7057) (Matthews et al., 1994) corresponding to the isotopic baseline values of MASH-magmas derived from the lower crust (0.705; sensu Davidson et al., 1990). Moreover, the selected sample has a low SiO_2 (~57 wt%) and Mg number (defined as 100MgO/(MgO + FeO)) in mole per cent) (Mg# = 51), similar to the BA end-member (Blum-Oeste and Wörner, 2016). As the contaminant, samples from the Paleozoic Andean basement we used a bulk felsic upper crustal composition of the zone that correspond to the northern Sierra de Moreno (Lucassen et al., 2001), which is exposed 60 NE of the SPLVC. Crustal rocks from this area have $^{87}Sr/^{86}Sr$ ratios ranging from 0.707 and 0.728, with SiO_2 values from 54 to 69 wt%, and Mg#·between 35 and 60 (Lucassen et al., 2001). For AFC-model calculations, the average Sr composition of Paleozoic crust was used. Also, a mineral assemblage was generated taking into account the petrographic characteristic of the lavas from the San Pedro – Linzor volcanic chain (O'Callaghan and Francis, 1986; Godoy et al., 2014; López, 2014; Martínez, 2014; Silva, 2015; Lazcano, 2016) (Table 5). The resulting models are plotted in Fig. 10a.

Results of RAFT-modeling (Aitcheson and Forrest, 1994; Table 6) indicate that the proportion of assimilated crust varies from ~12% to ~31%. For Toconce and Cerro del Leon, magma assimilation of crustal components varies between ~23% to ~31%. Lavas from Paniri assimilated between 12% and 23% of crustal material, while the calculated proportion of assimilated crustal material is lower at San Pedro volcano and La Poruña scoria cone, reaching up to ~13%. Thus, decreasing assimilation is observed from NW to SE along the SPLVC (Fig. 10a).

5.3. What is the role of the Altiplano-Puna Magmatic Body?

When we combine our new isotope and age data with previously published data in the region, systematic shifts in isotopic composition are recognized for lavas erupted during the past <2 Ma along a transect that crosses the western margin of the APMB (Fig. 10b). We will now consider the hypothesis that magmas maybe variably influenced by a crustal component derived from the APMB. The increase in radiogenic Sr observed in the NW-SE SPLVC (our data) towards the APMB is consistent with Sr isotope variations along transects from Ollagüe, and Aucanquilcha volcanoes to Uturuncu (Michelfelder et al., 2013) and (in a S to N direction) from Lascar volcano to Licancabur, Putana, and Sairecabur (using data compilation by Mamani et al., 2010; Fig. 10b).

Uturuncu volcano is located close to the center of the APMB (Fig. 1) and has the highest $^{87}Sr/^{86}Sr$, and lowest $^{143}Nd/^{144}Nd$ ratios (Muir et al.,

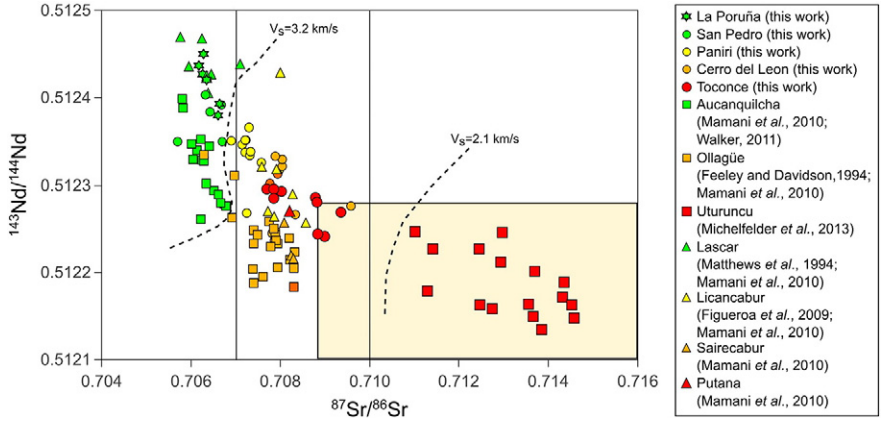

Fig. 9. $^{143}Nd/^{144}Nd$ vs. $^{87}Sr/^{86}Sr$ diagram for selected volcanic centres in the Central Andes. Dotted lines indicate joint ambient noise-receiver function inversion S-velocity models contours (V_s), at 15 km b.s.l., where seismic velocities < 2.1 km/s are indicative of the Altiplano-Puna magmatic body (APMB) (Ward et al., 2014). Square area represents values for ignimbrites of the Altiplano-Puna Volcanic Complex (data from Kay et al., 2010; Burns et al., 2015).

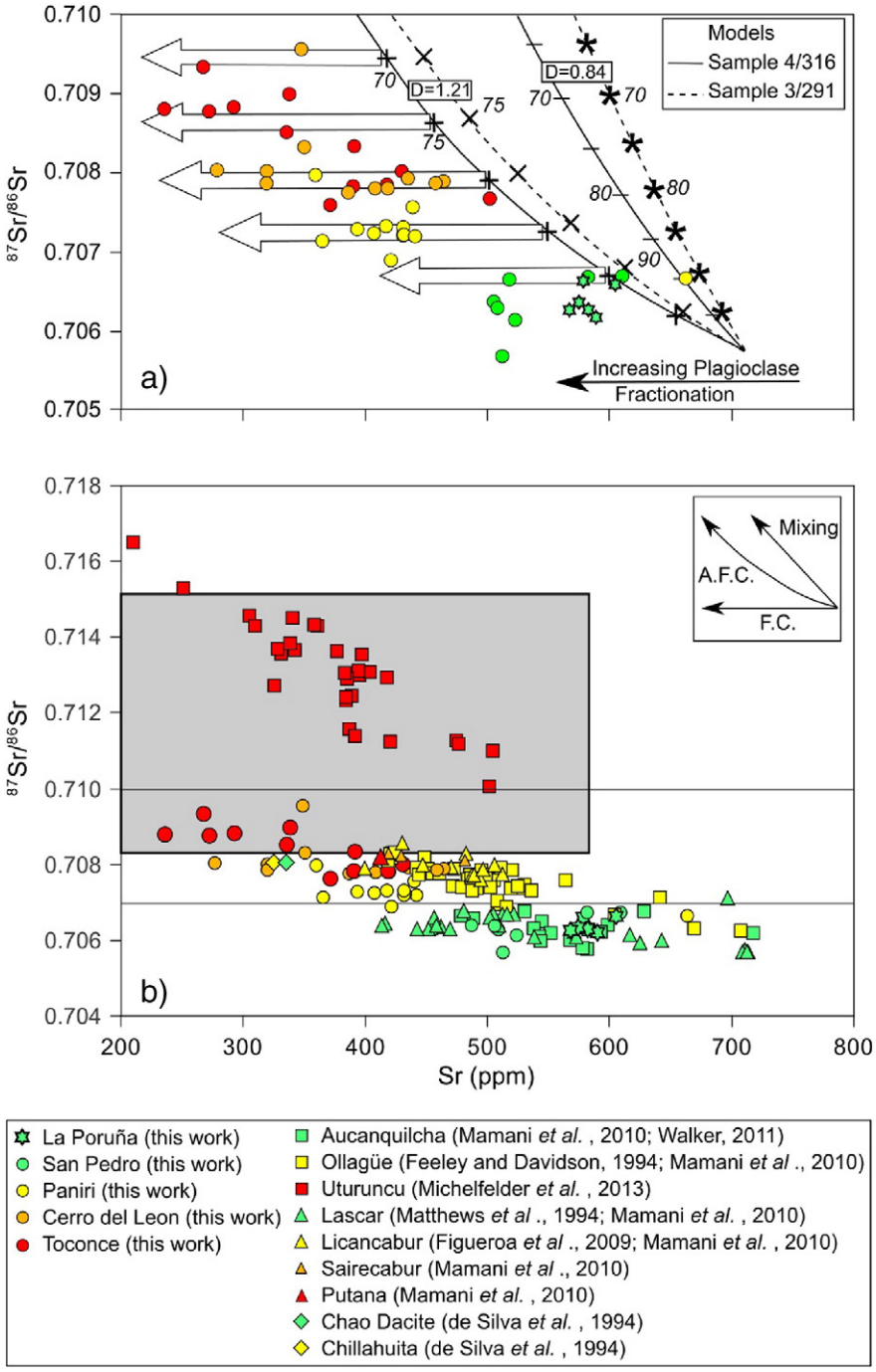

Fig. 10. $^{87}Sr/^{86}Sr$ vs Sr (ppm) diagram for a) analyzed samples from SPLVC (Table 1), and b) selected lavas erupted in the Central Andes. In a) white arrows represent proposed trends for closed system fractional crystallization starting from magmas that were initially formed by an AFC process (arrows widths are 0.002 on the $^{87}Sr/^{86}Sr$ ratio). Plotted AFC models according to data from Table 5. Numbers in italic indicate estimated remaining melt fraction (F, %). In b) lavas from Uturuncu lavas show a trend similar to a magma mixing model (inset), while those of Aucanquilcha and Lascar volcanoes show an almost horizontal trend similar to fractional crystallization (F.C.) models (inset). AFC in the inset corresponds to a plagioclase-dominated assimilation and fractional crystallization trend. Square area represents values for ignimbrites of the Altiplano-Puna Volcanic Complex (data from de Silva et al., 1994; Lindsay et al., 2001; Kay et al., 2010; Burns et al., 2015).

2014, 2015) of any andesitic magma in the active volcanic front (Fig. 9). The high Sr isotope ratios of Uturuncu andesites were related to mixing between mafic magmas and dacite magma derived from the APMB by interaction within a ~11 km thick vertical mush column (Muir et al., 2014, 2015). The radiogenic Sr and Nd isotope values of Uturuncu match those of the evolved, large volume ignimbrites in the southern CVZ (Fig. 9) and suggest large crustal contributions (Muir et al., 2014, 2015) that are similar to the crustal components of up to 60% have been proposed for APVC ignimbrites (Freymuth et al., 2015). In a transect from Uturuncu to the west towards Ollagüe, and Aucanquilcha volcanoes (Michelfelder et al., 2013) maximum Sr isotope ratios drop to 0.706, i.e. typical values for the volcanoes of the active front and beyond the western border of the APMB (Fig. 11). A similar compositional change with increasingly radiogenic Sr isotope signatures is observed in lavas along S-N transect from Lascar to Licancabur, Sairecabur and Putana (Figs. 9 and 10). In essence, volcanoes that are located close to, or outside the margins of the APMB (e.g. San Pedro, Aucanquilcha, Lascar volcanoes, La Poruña scoria cone), show consistently lower $^{87}Sr/^{86}Sr$ ratios, and higher $^{143}Nd/^{144}Nd$ ratios (Fig. 9), even in lavas with >65 wt% SiO_2.

Table 5
AFC-type model parameters (after DePaolo, 1981) for erupted magmas at San Pedro – Linzor volcanic chain. Bulk D according to partitioning coefficients from Rollinson (1993) for basaltic melts.[a]

	Initial	Contaminant		Mineral assemblage	(% vol)
Location	Lascar volcano	Sierra de Moreno		Plagioclase	40
Reference	Matthews et al. (1994)	Lucassen et al. (2001)		Clinopyroxene	30
Sample	LA 123	3/291	4/316	Orthopyroxene	15
SiO_2 (wt%)[a]	57.55	68.80	65.28	Hornblende	5
Al_2O_3 (wt%)[a]	17.10	13.41	15.12	Olivine	5
CaO (wt%)[a]	7.11	2.72	1.78		
Na_2O (wt%)[a]	3.64	3.20	2.47	D^{Sr} (bulk)	0.84
K_2O (wt%)[a]	1.55	1.64	3.19	D^{Nd} (bulk)	0.2
MgO (wt%)[a]	3.78	1.94	2.14		
FeO^t (wt%)[a]	6.36	5.93	5.63		
Sr (ppm)	711	271	185		
$^{87}Sr/^{86}Sr$	0.705765	0.721843	0.72777	Conditions	
Nd (ppm)	25	27	37	$r = M_a/M_c$	0.6
$^{143}Nd/^{144}Nd$	0.51247	0.511961	0.512087		

t = total Fe as Fe^{2+}.
[a] Recalculated 100% water free.

We propose that lateral variations in Sr- and Nd-isotope compositions of magmas erupted across the margin of the APMB are related to increased degrees of assimilation by this magmatic crustal body (Fig. 11), rather than by vertical or lateral heterogeneity of the crust. S-wave velocities indicate an increase in melt/fluid percentage from the margin of the partially molten APMB from ~4% for zones with S-velocities of 3.2 km/s, to ~10% (2.9 km/s), and up to 25% in zones with velocities <1.9 km/s (Figs. 1, 9, 11; Schilling et al., 1997; Zandt et al., 2003; Ward et al., 2014). Such differences in melt proportion within the APMB should result in variable degrees of interaction between ascending magmas coming from deeper sources and shallow partial crustal melts. Interaction between less differentiated magma and this crystal-rich mush increases from the border to the center of the mush-type zone as observed along the SPLVC (increasing from ~12 to ~31% assimilated crustal material; Table 6). At the center of the APMB, where assimilation is most significant (Fig. 11) magmas interact along the entire mush column (Muir et al., 2014, 2015) and become more assimilated by crustal melts. Towards the margin, less radiogenic arc magmas (e.g. Lascar and Aucanquilcha volcanoes) ascend from their deep source to the surface with increasingly less crustal interaction with the APMB (Fig. 11, Matthews et al., 1994; Walker et al., 2013).

Table 6
Calculated ρ and assimilated crust calculated using Eq. (5) by Aitcheson and Forrest (1994). Sr (ppm) and $^{87}Sr/^{86}Sr$ data according to analytical results (Table 1), and estimated remaining melt fraction (F) from AFC-type model using sample 4/316 (Table 4).

F (%)	Sr (ppm)	$^{87}Sr/^{86}Sr$	r (crust/magma ratio)	Assimilated crust (%)
90	601	0.70673	0.15	13.0
85	550	0.707302	0.23	18.4
80	502	0.707948	0.30	23.1
75	458	0.708675	0.37	27.2
70	416	0.709495	0.45	31.0
Sample				
BG-SPL-022[a]	663	0.706676	0.15	12.7
BG-SPL-010 (San Pedro)[b]	610	0.706705	0.14	12.2
POR 14 01 (La Poruña)[b]	608	0.706640	0.14	12.2

[a] Bulk partitioning (DSr) = 0.84.
[b] Bulk partitioning (DSr) = 1.21.

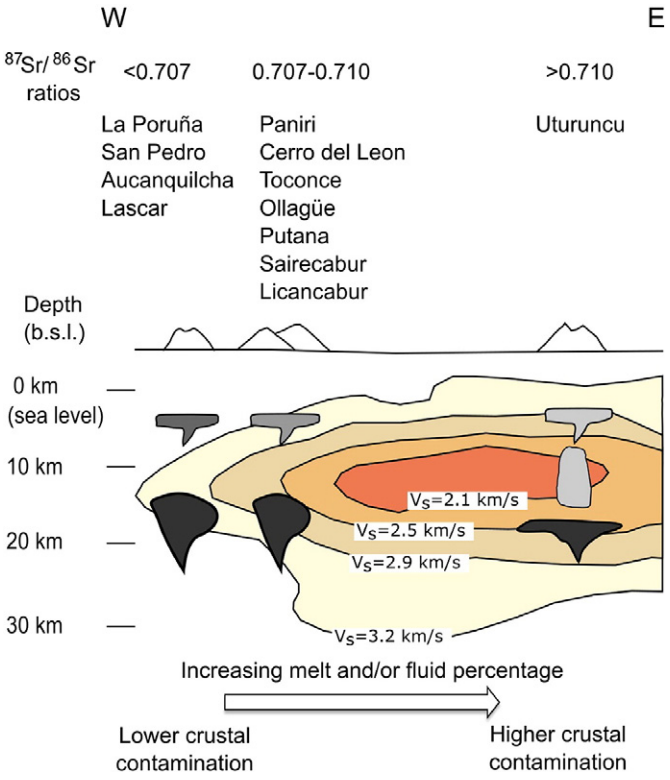

Fig. 11. Schematic cross section showing variation of crustal contamination at the Altiplano-Puna Volcanic Complex with cross-sections of the joint ambient noise-receiver function inversion S-velocity model from the C-C′ profile by Ward et al. (2014). Velocity contour lines of 3.2, 2.9, 2.5, and 2.1 km/s are shown. Magmatism closer to the APMB core with increasing melt/fluid percentages favors the interaction between mafic magmas and the upper crustal mush zone. At the center of the APMB, andesite magmas have $^{87}Sr/^{86}Sr$ ratios >0.710 (e.g. Uturuncu volcano) representing the highest proportion of crustal melts. Dark grey areas represent primary mafic magmas ascending from deeper sources. Shades of grey indicate extend of crustal contamination based on $^{87}Sr/^{86}Sr$ data. Upper magmatic chamber location according to data from Martínez (2014) and Muir et al. (2014).

6. Conclusions

The SPLVC has grown and evolved over the past 2 Ma, during the waning of the ignimbrite flare-up in the APVC. The chain developed across the western margin of the APMB, an upper crustal, partially molten zone with decreasing proportion of crustal melts towards its margins. Arc magmas that interacted with the lower crust prior to their ascent mixed with different proportions this upper-crustal melt zone (APMB) to explain the formation of magmas with variable radiogenic Sr and Nd isotope compositions. Similar increasing Sr-isotope ratios of between 0.709 and 0.707 are detected in transects across the margins of the APMB reaching maximum values (0.710–0.717) in lavas of Uturuncu volcano above the center of this partially molten zone. Volcanoes located outside the limits of the APMB (e.g. San Pedro-San Pablo, Aucanchilca, Lascar), are less radiogenic in Sr and similar to CVZ magmatism elsewhere. The lower degree of interaction with APMB crustal components from its transitional crystal-rich and cooler mush zones in the marginal of the APMB could explain the volcanoes with less radiogenic Sr isotope compositions (e.g. SPLVC, Aucanquilcha, Ollagüe). This behavior is independent of time as observed at Aucanquilcha and Lascar volcanoes which show similar low radiogenic signatures at different ages (Fig. 8). This indicates that the presence of the APMB has influenced the composition of erupted magmas for at least the last 2 M.y.

Essentially, there is a direct correlation between the Sr and Nd isotopic composition of erupted lavas at various stratovolcanoes and the AMPB seismic velocity structure within the crust that underlies them

(Figs. 9, 11). We consider this the strongest evidence for the fundamental role that the partial molten zone of the APMB excerts on the isotopic signature (and thus degree of crustal component) of erupted magmas along the arc front volcanoes. We also note the near absence of the enriched parent magma component in this particular area that was proposed by Blum-Oeste and Wörner (2016) to be an important magmatic component in Central Andean magmatism in general.

Acknowledgments

Authors thank Dr. Robert B. Trumbull, Dr. James Gardner, and an anonymous reviewer for helpful comments. We also thank Energía Andina S.A. for providing $^{40}Ar/^{39}Ar$ data. This work was funded by DGIP-UCN no 10301265, CONICYT no 24100002, FONDAP-CONICYT no 15090013, and CONICYT/FONDECYT Postdoctoral no 3160432 projects. O.G.-M. is a Ph.D. (c) granted by CONICYT-PCHA no 2015-21150403 scholarship.

References

Aitcheson, S.J., Forrest, A.H., 1994. Quantification of crustal contamination in open magmatic systems. J. Petrol. 35 (2):461–488. http://dx.doi.org/10.1093/petrology/35.2.461.

Allmendinger, R.W., Jordan, T.E., Kay, S.M., Isacks, B., 1997. The evolution of the Altiplano-Puna plateau of the Central Andes. Annu. Rev. Earth Planet. Sci. 25 (1):139–174. http://dx.doi.org/10.1146/annurev.earth.25.1.139.

Arancibia, G., Matthews, S.J., Perez de Arce, C., 2006. K–Ar and $^{40}Ar/^{39}Ar$ geochronology of supergene processes in the Atacama Desert, Northern Chile: tectonic and climatic relations. J. Geol. Soc. Lond. 63 (1):107–118. http://dx.doi.org/10.1144/0016-764904-161.

Baker, M.C.W., Francis, P.W., 1978. Upper Cenozoic volcanism in the Central Andes – ages and volumes. Earth Planet. Sci. Lett. 41 (2):175–187. http://dx.doi.org/10.1016/0012-821X(78)90008-0.

Beck, S.L., Zandt, G., Myers, S.C., Wallace, T.C., Silver, P.G., Drake, L., 1996. Crustal thickness variations in the central Andes. Geology 24 (5):407–410. http://dx.doi.org/10.1130/0091-7613.

Blum-Oeste, M., Wörner, G., 2016. Central Andean magmatism can be constrained by three ubiquitous end-members. Terra Nova 28 (6):434–440. http://dx.doi.org/10.1111/ter.12237.

Brandmeier, M., Wörner, G., 2016. Compositional variations of ignimbrite magmatism in the Central Andes over the past 26 Ma - a multivariate statistical perspective. Lithos 262:713–728. http://dx.doi.org/10.1016/j.lithos.2016.07.011.

Brasse, H., Lezaeta, P., Rath, V., Schwalenberg, K., Soyer, W., Haak, V., 2002. The Bolivian Anltiplano conductivity anomaly. J. Geophys. Res. 107 (B5):2096. http://dx.doi.org/10.1029/2001JB000391.

Burns, D.H., de Silva, S.L., Tepley III, F., Schmitt, A.K., Loewen, M.W., 2015. Recording the transition from flare-up to steady-state arc magmatism at the Purico-Chascon volcanic complex, northern Chile. Earth Planet. Sci. Lett. 422:75–86. http://dx.doi.org/10.1016/j.epsl.2015.04.002.

Caffe, P.J., Trumbull, R.B., Coira, B.L., Romer, R.L., 2002. Petrogenesis of Early Neogene magmatism in the Northern Puna; implications from magma genesis and crustal processes in the Central Andean Plateau. J. Petrol. 43 (5):907–942. http://dx.doi.org/10.1093/petrology/43.5.907.

Chmielowski, J., Zandt, G., Haberland, C., 1999. The Central Andean Altiplano-Puna magma body. Geophys. Res. Lett. 26 (6):783–786. http://dx.doi.org/10.1029/1999GL900078.

Coira, B., Davidson, J., Mpodozis, C., Ramos, V., 1982. Tectonic and magmatic evolution of the Andes of Northern Argentina and Chile. Earth Sci. Rev. 18 (3-4):303–332. http://dx.doi.org/10.1016/0012-8252(82)90042-3.

Davidson, J.P., McMillan, N.J., Moorbath, S., Wörner, G., Harmon, R.S., López-Escobar, L., 1990. The Nevados de Payachata volcanic region (18_S/69_W, N. Chile) II. Evidence for widespread crustal involvement in Andean magmatism. Contrib. Mineral. Petrol. 105 (4):412–432. http://dx.doi.org/10.1007/BF00286829.

Delunel, R., Blard, P.H., Martin, L.C.P., Nomade, S., Schlunegger, F., 2016. Long term low latitude and high elevation cosmogenic ^{3}He production rate inferred from a 107 ka-old lava flow in northern Chile; 22°S–3400 m a.s.l. Geochim. Cosmochim. Acta 184:71–87. http://dx.doi.org/10.1016/j.gca.2016.04.023.

DePaolo, D.J., 1981. Trace element and isotopic effects of combined wallrock assimilation and fractional crystallization. Earth Planet. Sci. Lett. 53 (2):189–202. http://dx.doi.org/10.1016/0012-821X(81)90153-9.

Feeley, T.C., Davidson, J.P., 1994. Petrology of calc-alkaline lavas at Volcán Ollagüe and the origin of compositional diversity at Central Andean stratovolcanoes. J. Petrol. 35 (5):1295–1340. http://dx.doi.org/10.1093/petrology/35.5.1295.

Figueroa, O., Déruelle, B., Demaiffe, D., 2009. Genesis of adakite-like lavas of Licancabur volcano (Chile—Bolivia, Central Andes). Compt. Rendus Geosci. 341 (4):310–318. http://dx.doi.org/10.1016/j.crte.2008.11.008.

Freymuth, H., Brandmeier, M., Wörner, G., 2015. The origin and crust/mantle mass balance of Central Andean ignimbrite magmatism constrained by oxygen and strontium isotopes and erupted volumes. Contrib. Mineral. Petrol. 169 (6):1–24. http://dx.doi.org/10.1007/s00410-015-1152-5.

Frimmel, H.E., Zartman, R.E., Späth, A., 2001. Dating Neoproterozoic continental break-up in the Richtersveld Igneous Complex, South Africa. J. Geol. 109 (4):493–508. http://dx.doi.org/10.1086/320795.

Gardeweg, M., Amigo, A., Matthews, S.J., Sparks, R.S.J., Clavero, J., 2011. Geología del Volcán Láscar, Región de Antofagasta. Carta Geológica de Chile, Serie Geología Básica, No 131, escala 1:50000. Servicio Nacional de Geología y, Minería, Chile.

Global Volcanism Program, 2013. http://www.volcano.si.edu/volcano.cfm?vn=355070.

Godoy, B., Wörner, G., Kojima, S., Aguilera, F., Simon, K., Hartmann, G., 2014. Low-pressure evolution of arc magmas in thickened crust: the San Pedro-Linzor volcanic chain, Central Andes, Northern Chile. J. S. Am. Earth Sci. 52:24–42. http://dx.doi.org/10.1016/j.jsames.2014.02.004.

Grocke, S.B., Cottrella, E., de Silva, S., Kelley, K.A., 2016. The role of crustal and eruptive processes versus source variations in controlling the oxidation state of iron in Central Andean magmas. Earth Planet. Sci. Lett. 440:92–104. http://dx.doi.org/10.1016/j.epsl.2016.01.026.

Grove, T.L., Till, C.B., Krawczynski, M.J., 2012. The Role of H_2O in Subduction Zone Magmatism. Annu. Rev. Earth Planet. Sci. 40 (1):413–439. http://dx.doi.org/10.1146/annurev-earth-042711-105310.

Grunder, A.L., Klemetti, E.K., McKee, C.M., Feeley, T.C., 2006. Eleven million years of arc volcanism at the Aucanquilcha volcanic cluster, Northern Chilean Andes: implications for the lifespan and emplacement of batholiths. Trans. R. Soc. Edinb. Earth Sci. 97 (4):415–436. http://dx.doi.org/10.1017/S0263593300001541.

Guest, J.E., Sanchez, J., 1969. A large dacitic lava flow in Northern Chile. Bull. Volcanol. 33 (3):778–790. http://dx.doi.org/10.1007/BF02596749.

Haberland, C., Rietbrock, A., 2001. Attenuation tomography in the western central Andes: A detailed insight into the structure of a magmatic arc. J. Geophys. Res. 106 (B6):11151–11167. http://dx.doi.org/10.1029/2000JB900472.

Harris, C., le Roux, P.J., Cochrane, R., Martin, L., Duncan, A.R., Marsh, J.S., le Roex, A.P., Class, C., 2015. The oxygen isotope composition of Karoo and Etendeka picrites: High δ18O mantle or crustal contamination? Contrib. Mineral. Petrol. 170:8. http://dx.doi.org/10.1007/s00410-015-1164-1.

Hartley, A.J., Sempere, T., Wörner, G., 2007. A comment on "Rapid late Miocene rise of the Bolivian Altiplano: evidence for removal of mantle lithosphere" by Garzione C.N. et al. [Earth Planet. Sci Lett. 241 (2006) 543–556]. Earth Planet. Sci. Lett. 259(3/4):625–629. http://dx.doi.org/10.1016/j.epsl.2007.04.012.

Haschke, M.R., 2002. Evolutionary Geochemical Patterns of Late Cretaceous to Eocene arc Magmatic Rocks in North Chile: Implications for Archean Crustal Growth. 2. EGU Stephan Mueller Special Publication Series:pp. 207–218. http://dx.doi.org/10.5194/smsps-2-207-2002.

Haschke, M., Günther, A., Melnick, D., Echtler, H., Reutter, K.-J., Scheuber, E., Oncken, O., 2006. Central and Southern Andean tectonic evolution inferred from arc magmatism. In: Oncken, O., Chong, G., Franz, G., Giese, P., Götze, H.-J., Ramos, V.A., Strecker, M.R., Wigger, P. (Eds.), The Andes Active Subduction Orogeny, Frontiers in Earth Sciences. 1. Springer, Heidelberg, Berlin, Germany:pp. 337–353. http://dx.doi.org/10.1007/978-3-540-48684-8_16.

Hildreth, W., 1981. Gradients in silicic magma chambers: implications for lithospheric magmatism. J. Geophys. Res. 86 (B11):10153–10192. http://dx.doi.org/10.1029/JB086iB11p10153.

Irvine, T.N., Baragar, W.R.A., 1971. A guide to the chemical classification of the common volcanic rocks. Can. J. Earth Sci. 8 (5):523–548. http://dx.doi.org/10.1139/e71-055.

Kay, S.M., Mpodozis, C., 2001. Central Andean ore deposits linked to evolving shallow subduction systems and thickening crust. GSA Today 11 (3), 4–9.

Kay, S.M., Godoy, E., Kurtz, A., 2005. Episodic arc migration, crustal thickening, subduction erosion, and magmatism in the south-central Andes. Geol. Soc. Am. Bull. 117 (1/2):67–88. http://dx.doi.org/10.1130/B25431.1.

Kay, S.M., Coira, B.L., Caffe, P.J., Chen, C.-H., 2010. Regional chemical diversity, crustal and mantle sources and evolution of central Andean Puna plateau ignimbrites. J. Volcanol. Geotherm. Res. 198 (1–2):81–111. http://dx.doi.org/10.1016/j.jvolgeores.2010.08.013.

Kern, J.M., de Silva, S.L., Schmitt, A.K., Kaiser, J.F., Iriarte, A.R., Economos, R., 2016. Geochronological imaging of an episodically constructed subvolcanic batholith: U-Pb in zircon chronochemistry of the Altiplano-Puna Volcanic Complex of the Central Andes. Geosphere 12 (4):1–24. http://dx.doi.org/10.1130/GES01258.1.

Klemetti, E.W., Grunder, A.L., 2008. Volcanic evolution of Volcán Aucanquilcha: a long-lived dacite volcano in the Central Andes of northern Chile. Bull. Volcanol. 70 (5):633–650. http://dx.doi.org/10.1007/s00445-007-0158-x.

Kley, J., Monaldi, C.R., 1998. Tectonic shortening and crustal thickness in the Central Andes: how good is the correlation? Geology 26 (8):723–726. http://dx.doi.org/10.1130/0091-7613.

Kley, J., Monaldi, C.R., Salfity, J.A., 1999. Along-strike segmentation of the Andean foreland: causes and consequences. Tectonophysics 301 (1–2):75–94. http://dx.doi.org/10.1016/S0040-1951(98)90223-2.

Koppers, A.A.P., Staudigel, H., Duncan, R.A., 2003. High-resolution Ar-^{40}/Ar-39 dating of the oldest oceanic basement basalts in the western Pacific basin. Geochem. Geophys. Geosyst. 4 (11):8914. http://dx.doi.org/10.1029/2003GC000574.

Lazcano, J., 2016. Evolución volcanológica del Volcán Paniri (Región de Antofagasta, Chile). (Dissertation, Bachelor's Degree Thesis). Universidad Católica del Norte, Antofagasta, Chile.

Lazcano, J., Godoy, B., Aguilera, F., Wilke, H.G., 2012. Volcanological Evolution of Paniri Volcano, Central Andes, Northern Chile. AGU Fall Meeting, Abstracts, San Francisco, USA, pp. V21A–2759 (December).

Le Maitre, R.W., 1984. A proposal by the IUGS Subcommission on the Systematics of Igneous Rocks for a chemical classification of volcanic rocks based on the total alkali silica (TAS) diagram. Aust. J. Earth Sci. 31 (2):243–255. http://dx.doi.org/10.1080/08120098408729295.

Lindsay, J.M., Schmitt, A.K., Trumbull, R.B., de Silva, S.L., Siebel, W., Emmermann, R., 2001. Magmatic evolution of the La Pacana caldera system, Central Andes, Chile:

compositional variations of two cogenetic large-volume felsic ignimbrites. J. Petrol. 42 (3):459–486. http://dx.doi.org/10.1093/petrology/42.3.459.
López, C., 2014. Evolucion geológica del Volcan Toconce, Region de Antofagasta, Chile. (Dissertation, Bacherlor's Degree Thesis). Universidad de Atacama, Copiapo, Chile.
López, C., Aguilera, F., Godoy, B., Wörner, G., Kojima, S., 2012. Evolución del sistema volcánico Toconce (Región de Antofagasta, Chile) mediante interpretación fotogeológica, petrográfica y geoquímica. T4. XII Congreso Geológico Chileno, Antofagasta, Chile, pp. 594–596.
Lucassen, F., Becchio, R., Harmon, R., Kasemann, S., Franz, G., Trumbull, R., Wilke, H.-G., Romer, R.L., Dulski, P., 2001. Composition and density model of the continental crust at an active continental margin – the Central Andes between 21° and 27°S. Tectonophysics 341 (1–4):195–223. http://dx.doi.org/10.1016/S0040-1951(01)00188-3.
Ludwig, K.R., 2012. Isoplot, A Geochronological Toolkit for Microsoft Excel. Berkeley Geochronology Center (Special Publication No. 5, 75 pp.).
Mamani, M., Tassara, A., Wörner, G., 2008. Composition and structural control of crustal domains in the Central Andes. Geochem. Geophys. Geosyst. 9 (3), Q03006. http://dx.doi.org/10.1029/2007GC001925.
Mamani, M., Wörner, G., Sempere, T., 2010. Geochemical variations in igneous rocks of the Central Andean orocline (13°S to 18°S): tracking crustal thickening and magma generation through time and space. Geol. Soc. Am. Bull. 122 (1/2):162–182. http://dx.doi.org/10.1130/B26538.1.
Marinovic, N., Lahsen, A., 1984. Carta Geológica de Chile, Hoja Calama, Escala 1: 250.000. Carta No 58. Servicio Nacional de Geología y Minería, Santiago, Chile.
Martínez, P., 2014. Petrologia y geoquímica de lavas recientes, al noroeste del Campo Geotermal del Tatio. (Dissertation, Bachelor's Degree Thesis). Universidad de Chile, Santiago, Chile.
Matthews, S.J., Jones, A.P., Gardeweg, M.C., 1994. Lascar Volcano, Northern Chile; evidence for steady-state disequilibrium. J. Petrol. 35 (2):401–432. http://dx.doi.org/10.1093/petrology/35.2.401.
McMillan, N., Davidson, J., Wörner, G., Harmon, R.S., Lopez-Escobar, L., Moorbath, S., 1993. Influence of crustal thickening on arc magmatism: Nevados de Payachata Region, northern Chile. Geology 21:467–470. http://dx.doi.org/10.1130/0091-7613(1993)021<0467:IOCTOA>2.3.CO;2.
Michelfelder, G.S., Feeley, T.C., Wilder, A.D., Klemetti, E.W., 2013. Modification of the continental crust by subduction zone magmatism and vice-versa: across-strike geochemical variations of silicic lavas from individual eruptive centers in the Andean central volcanic zone. Geosciences 3 (4):633–667. http://dx.doi.org/10.3390/geosciences3040633.
Muir, D.D., Blundy, J.D., Hutchinson, M.C., Rust, A.C., 2014. Petrological imaging of an active pluton beneath Cerro Uturuncu, Bolivia. Contrib. Mineral. Petrol. 167:980. http://dx.doi.org/10.1007/s00410-014-0980-z.
Muir, D.D., Barfod, D.N., Blundy, J.D., Rust, A.C., Sparks, R.S.J., Clarke, K.M., 2015. The temporal record of magmatism at Cerro Uturuncu, Bolivian Altiplano. In: Caricchi, L., Blundy, J.D. (Eds.), Chemical, Physical, and Temporal Evolution of Magmatic Systems. 422(1). Geological Society of London Special Publications:pp. 57–82. http://dx.doi.org/10.1144/SP422.1.
O'Callaghan, L.J., Francis, P.W., 1986. Volcanological and petrological evolution of San Pedro volcano, Provincia El Loa, North Chile. J. Geol. Soc. Lond. 143 (2):275–286. http://dx.doi.org/10.1144/gsjgs.143.2.0275.
Oncken, O., Hindle, D., Kley, J., Elger, K., Victor, P., Schemmann, K., 2006. Deformation of the Central Andean upper plate system e facts, fiction, and constraints for plateau models. In: Oncken, O., Chong, G., Franz, G., Giese, P., Götze, H.-J., Ramos, V.A., Strecker, M.R., Wigger, P. (Eds.), The Andes Active Subduction Orogeny, Frontiers in Earth Sciences. 1. Springer, Heidelberg, Berlin, Germany:pp. 3–27. http://dx.doi.org/10.1007/978-3-540-48684-8_1.
Ort, M.H., Coira, B.L., Mazzoni, M.M., 1996. Generation of a crust-mantle magma mixture: magma sources and contamination at Cerros Panizos, central Andes. Contrib. Mineral. Petrol. 123 (3):308–322. http://dx.doi.org/10.1007/s004100050158.
Polanco, E., Clavero, J., Giaveli, A., 2012. Geología de la cadena volcánica Paniri-Toconce, Zona Volcánica Central, Altiplano de la Región de Antofagasta, Chile. T4. XII Congreso Geológico Chileno, Antofagasta, Chile, pp. 462–464.
Prezzi, C.B., Götze, H.-J., Schmidt, S., 2009. 3D density model of the Central Andes. Phys. Earth Planet. Inter. 177 (3–4):217–234. http://dx.doi.org/10.1016/j.pepi.2009.09.004.
Ramírez, C., Huete, C., 1981. Carta Geológica de Chile, Hoja Ollagüe. Escala 1: 250.000. Carta No 40. Instituto de Investigaciones Geológicas, Santiago, Chile.
Rogers, G., Hawkesworth, C.J., 1989. A geochemical traverse across the North Chilean Andes: evidence for crust generation from the mantle wedge. Earth Planet. Sci. Lett. 91 (3/4):271–285. http://dx.doi.org/10.1016/0012-821X(89)90003-4.
Rollinson, H.R., 1993. Using Geochemical Data: Evaluation, Presentation, Interpretation. Longman Scientific and Technical (352 pp.).
Salisbury, M.J., Jicha, B.R., de Silva, S.L., Singer, B.S., Jiméez, N.C., Ort, M.H., 2011. $^{40}Ar/^{39}Ar$ chronostratigraphy of Altiplano-Puna volcanic complex ignimbrites reveals the development of a major magmatic province. Geol. Soc. Am. Bull. 123 (5/6):821–840. http://dx.doi.org/10.1130/B30280.1.
Scheuber, E., Giese, P., 1999. Architecture of the Central Andes - a compilation of geoscientific data along a transect at 21°S. J. S. Am. Earth Sci. 12 (2):103–107. http://dx.doi.org/10.1016/S0895-9811(99)00008-5.
Scheuber, E., Reutter, K.-J., 1992. Magmatic arc tectonics in the Central Andes between 21°and 25°S. Tectonophysics 205 (1–3):127–140. http://dx.doi.org/10.1016/0040-1951(92)90422-3.
Schilling, F.R., Partzsch, G.M., 2001. Quantifying partial melt fraction in the crust beneath the Central Andes and the Tibetan Plateau. Phys. Chem. Earth A 26 (4–5):239–246. http://dx.doi.org/10.1016/S1464-1895(01)00051-5.
Schilling, F.R., Partzsch, G.M., Brasse, H., Schwarz, G., 1997. Partial melting below the magmatic arc in the central Andes deduced from geoelectromagnetic field experiments and laboratory data. Phys. Earth Planet. Inter. 103 (1–2):17–31. http://dx.doi.org/10.1016/S0031-9201(97)00011-3.
Schmitt, A.K., de Silva, S.L., Trumbull, R.B., Emmermann, R., 2001. Magma evolution in the Purico ignimbrite complex, northern Chile: Evidence for zoning of a dacitic magma by injection of rhyolitic melts following mafic recharge. Contrib. Mineral. Petrol. 140 (6):680–700. http://dx.doi.org/10.1007/s004100000214.
Schnurr, W.B.W., Trumbull, R.B., Clavero, J., Hahne, K., Siebel, W., Gardeweg, M., 2007. Twenty-five million years of silicic volcanism in the southern central volcanic zone of the Andes: Geochemistry and magma genesis of ignimbrites from 25 to 27°S, 67 to 72°W. J. Volcanol. Geotherm. Res. 166 (1):17–46. http://dx.doi.org/10.1016/j.jvolgeores.2007.06.005.
Seelenfreund, A., Fonseca, E., Llona, F., Lera, L., Sinclaire, C., Rees, C., 2009. Geochemical analysis of vitreous rocks exploited during the formative period in the Atacama region, northern Chile. Archaeometry 51 (1):1–25. http://dx.doi.org/10.1111/j.1475-4754.2008.00386.x.
de Silva, S.L., 1989. Altiplano-Puna volcanic complex of the central Andes. Geology 17 (12):1102–1106. http://dx.doi.org/10.1130/0091-7613.
Silva, F., 2015. Evolucion geológica del Volcán Cerro del León, Region de Antofagasta, Chile. (Dissertation, Bachelor's Degree Thesis). Universidad de Atacama, Copiapo, Chile.
de Silva, S.L., Francis, P.W., 1991. Volcanoes of the Central Andes. Springer-Verlag, Berlin (218 pp.).
de Silva, S.L., Gosnold, W.D., 2007. Episodic construction of batholiths: Insights from the spatiotemporal development of an ignimbrite flare-up. J. Volcanol. Geotherm. Res. 167 (1–4):320–335. http://dx.doi.org/10.1016/j.jvolgeores.2007.07.015.
de Silva, S.L., Self, S., Francis, P.W., Drake, R.E., Ramírez, C., 1994. Effusive silicic volcanism in the Central Andes: the Chao dacite and other young lavas of the Altiplano-Puna volcanic complex. J. Geophys. Res. 99 (B9):17805. http://dx.doi.org/10.1029/94JB00652.
de Silva, S.L., Zandt, G., Trumbull, R., Viramonte, J., 2006. Large scale silicic volcanism - the result of thermal maturation of the crust. In: Chen, Y.-T. (Ed.), Advances in Geosciences. World Scientific Press, pp. 215–230.
Silva, F., Aguilera, F., Godoy, B., Wörner, G., Kojima, S., 2012. Evolución del sistema volcánico Cerro del León (Región de Antofagasta, Chile) mediante interpretación fotogeológica, petrográfica y geoquímica. T4. XII Congreso Geológico Chileno, Antofagasta, Chile, pp. 597–599.
Sparks, R.S.J., Folkes, C.B., Humphreys, M.C.S., Barfod, D.N., Clavero, J., Sunagua, M.C., McNutt, S.R., Prichtard, M.E., 2008. Uturuncu Volcano, Bolivia: Volcanic unrest due to midcrustal magma intrusion. Am. J. Sci. 308 (6):727–769. http://dx.doi.org/10.2475/06.2008.01.
Stern, C.R., 2004. Active Andean volcanism: Its geologic and tectonic setting. Revista Geologica de Chile 31 (2):161–206. http://dx.doi.org/10.4067/S0716-02082004000200001.
Tatsumi, Y., Sakuyama, M., Fukuyama, H., 1983. Generation of arc basalt magmas and thermal structure of the mantle wedge in subduction zones. J. Geophys. Res. 88 (B7), 5815–5825.
Tibaldi, A., Corazzato, C., Rovida, A., 2009. Miocene-Quaternary structural evolution of the Uyuni-Atacama region, Andes of Chile and Bolivia. Tectonophysics 471 (1–2):114–135. http://dx.doi.org/10.1016/j.tecto.2008.09.011.
Tierney, C.R., Schmitt, A.K., Lovera, O.M., de Silva, S.L., 2016. Voluminous plutonism during volcanic quiescence revealed by thermochemical modeling of zircon. Geology 44 (8):683–686. http://dx.doi.org/10.1130/G37968.1.
Trumbull, R., Riller, U., Oncken, O., Scheuber, E., Munier, K., Hongn, F., 2006. The timeespace distribution of cenozoic volcanism in the South-Central Andes: a new data compilation and some tectonic implications. In: Oncken, O., Chong, G., Franz, G., Giese, P., Götze, H.-J., Ramos, V.A., Strecker, M.R., Wigger, P. (Eds.), The Andes Active Subduction Orogeny, Frontiers in Earth Sciences. 1. Springer, Heidelberg, Berlin, Germany:pp. 29–43. http://dx.doi.org/10.1007/978-3-540-48684-8_2.
Walker Jr., B.A., 2011. The Geochemical Evolution of the Aucanquilcha Volcanic Cluster: Prolonged Magmatism and its Crustal Consequences. (Dissertation, Ph.D. Thesis). Oregon State University, Corvallis, Oregon, USA.
Walker, B.A., Klemetti, E.W., Grunder, A.L., Dilles, J.H., Tepley, F.J., Giles, D., 2013. Crystal reaming during the assembly, maturation, and waning of an eleven-million-year crustal magma cycle: thermobarometry of the Aucanquilcha Volcanic Cluster. Contrib. Mineral. Petrol. 165 (4):663–682. http://dx.doi.org/10.1007/s00410-012-0829-2.
Ward, K.M., Zandt, G., Beck, S.L., Christensen, D.H., McFarlin, H., 2014. Seismic imaging of the magmatic underpinnings beneath the Altiplano-Puna volcanic complex from the joint inversion of surface wave dispersion and receiver functions. Earth Planet. Sci. Lett. 404:43–53. http://dx.doi.org/10.1016/j.epsl.2014.07.022.
Watts, R.B., de Silva, S.L., Jimenez de Rios, G., Croudace, I., 1999. Effusive eruption of viscous silicic magma triggered and driven by recharge: A case study of the Cerro Chascon-Tuntu Jarita Dome Complex in Southwest Bolivia. Bull. Volcanol. 60 (4):241–264. http://dx.doi.org/10.1007/s004450050274.
Wörner, G., Moorbath, S., Harmon, R.S., 1992. Andean Cenozoic volcanics reflect basement isotopic domains. Geology 20 (12):1103–1106. http://dx.doi.org/10.1130/0091-7613(1992)020<1103:ACVCRB>2.3.CO;2.
Wörner, G., Hammerschmidt, K., Henjes-Kunst, F., Lezaun, J., Wilke, H., 2000. Geochronology ($^{40}Ar/^{39}Ar$, K-Ar and He-exposure ages) of Cenozoic magmatic rocks from northern Chile (18 22°S): Implications for magmatism and tectonic evolution of the central Andes. Rev. Geol. Chile 27 (2):205–240. http://dx.doi.org/10.4067/S0716-02082000000200004.
Zandt, G., Leidig, M., Chmielowski, J., Baumont, D., Yuan, X., 2003. Seismic detection and characterization of the Altiplano-Puna magma body, Central Andes. Pure Appl. Geophys. 160 (3):789–807. http://dx.doi.org/10.1007/PL00012557.